# Dynamic Response of Flexible Viscoelastic Kerf Structures of Freeform Shapes

Zaryab Shahid[1], Coleman Gustav Bond[1], Molly Saylor Johnson[1], James E. Hubbard Jr.[1], Negar Kalantar[2] and Anastasia Muliana[1]
[1]Department of Mechanical Engineering, Texas A&M University
[2]California College of the Arts & the Texas A&M University System
Corresponding author: amuliana@tamu.edu

## Abstract

Kerfing which is also known as relief cutting is a technique used to create flexible freeform surfaces out of rigid planar surfaces. Due to their pleasing aesthetics, flexibility, and ability to be molded into desired freeform shapes, they have several potential applications in engineering and architecture. The flexibility and reconfigurability of kerf structures depend on several kerf parameters such as cut density, size of the unit cell, cut thickness, cut pattern, etc. This study focuses on using kerf structures to create freeform surfaces and understanding their dynamic response in terms of mode shapes, resonance frequencies, and stress wave propagation of reconfigurable large-scale kerf structures. The effect of kerf cut density and unit cell size on the unit-cell modal behaviors is first investigated using both mathematical modeling and experiments. A beam element model is used to capture deformations of kerf structures. Next, the shape reconfigurable behaviors of two kerf panels with uniform cut density and transitioning cut density are presented. The dynamic response of these two kerf panels is then examined. The analysis of large-scale kerf panels demonstrated the capability of the beam element model to capture the modal response of kerf panels. The flexibility of the kerf panels enables local and global shape reconfigurations, which can alter the dynamic response (i.e., modal response and stress wave propagation) of the kerf panels. We perform a comparative study on the effect of shape reconfiguration (local and global) on the modal response and stress propagation behavior of the kerf panel. Overall, these findings would help design kerf structures for indoor and outdoor architectures with desired performance requirements.

## 1. Introduction

Complex freeform structures have been widely used in many engineering structures from aerospace, civil, mechanical, and biomedical engineering. In addition to their aesthetic requirements, architectural and civil structures need to meet both functional and performance requirements [1]. For instance, the design of the freeform architecture for facades of buildings involves counteracting the wind pressure acting on the structures [2]. Similarly, freeform structures designed for indoor architecture affect the room acoustic characteristics [3-5].

This study focuses on the use of kerf panels in creating complex freeform surfaces and the understanding of the dynamic response- of kerf structures of freeform shapes. Kerfing is a method, which involves cutting or removing material to create locally flexible structures from relatively stiff planar mass-produced materials such as composite woods, metals, and alloys. With the kerfing technique, the structures can be morphed into any desired shape with controlled anisotropy and flexibility [6], [7, 8]. The kerf structures enable reconfigurability in terms of bending and twisting about multiple axes [9, 10]. Due to their flexibility, the kerf structures are easily molded into various complex geometries (see **Fig. 1**). These large-scale kerf structures are made of repeatable kerf unit cells cut with a specific kerf pattern and kerf cut density, which determines the flexibility behavior of kerf structures.

**Fig 1. Large-scale kerf structures made up of repeatable kerf unit cells**

Chen et al. recently studied the static deformation behaviors such as stretching, bending, and twisting in the segments of kerf unit cells cut with different kerf densities and kerf patterns [11]. The desired freeform flexible geometry can be achieved by varying kerf cut patterns and densities. Shahid et al. investigated the dynamic response (mode shapes, frequencies, stress wave propagation) of stand-alone single kerf unit-cell of a fixed size made of two materials, which are elastic steel and viscoelastic wood. They presented a viscoelastic beam element to model the kerf unit-cell, comprising of segmental straight beams. They concluded that the cross-sectional geometry of beams in the kerf unit cell controls the mode shapes and magnitude of resonant frequencies, while the mechanical properties of the materials affect only the resonant frequencies [12]. The combination of kerf unit cells forms large-scale kerf structures. By understanding the effect of kerf parameters (cut pattern, cut density, cell size, and arrangement) on the dynamic response of kerf panels, it is possible to create freeform shapes whose corresponding dynamics response can be controlled, which is the focus of the present study.

More common techniques to create complex geometries from planar materials are origami and kirigami [13]. The origami and kirigami structures rely on the principle of creating folds to morph them into different shapes, which work well for very thin (often referred to as zero-thickness) surfaces, and hence limit their applications. Origami and kirigami on finite thickness materials often lead to intricate hinge design and compromised shape of fold regions [14, 15], and are labor-intensive and cumbersome processes [16]. Whereas, the shape configuration in kerf structures depends on fundamental kerf parameters such as kerf cut density, kerf pattern, size of the unit cell, etc., which are relatively easier to manipulate to achieve desired complex shapes. The kerf structures can be formed out of stiff planar materials of finite thickness. The continuous flow of solid elements enables these structures to go into both microscopic (within a cell) and macroscopic (surface) shape changes [12]. The practicality

and ease of manufacturability of kerf structures can potentially lead to wider applications for indoor and outdoor architectures, adaptive structures, biomedical devices, etc.

Two-dimensional lattice structures are also known for their ability to achieve desired freeform shapes from planar surfaces. Similar to kerf structures they are used for their shape-morphing capability [17]. Despite both lattice and kerf structures being formed based on arrangements of unit cells, there is a notable difference between the lattice and kerf structures. The lattice structures are typically formed by closed single cells [12, 18, 19], whereas the kerf structures have unit cells comprising a continuous flow of slender elements [6]. The lattice structures are difficult to fabricate using single planar construction materials (e.g., metal, wood, and polymer sheets) without generating lots of waste. A 3D printing or mold casting is needed to form lattice structures of various customized cell shapes and sizes. The kerf structures are more flexible to manufacture: they can be cut out of planar construction materials or 3D printed. However, lattice structures offer a significant weight reduction than kerf structures.

There have been numerous studies on comprehending the dynamic response in origami, kirigami, and lattice structures. The local characteristics such as facet's elasticity and fold properties are considered important in predicting the dynamics response of origami and kirigami structures. Based on their importance, structural models have been developed to investigate the effect of the geometry of facets, angles of the fold, and material properties of the facets on the modal response of origami and kirigami structures [20, 21]. On the other hand, the lattice structures made up of individual segments of beam elements are commonly used to model their dynamics response, e.g., [22], [23], and [24]. In the case of experiments, Popescu [25] and Bilal et al. [26] used laser vibrometry to study the modal response of lattice structures, which will be used for experiments on kerf structures in our study.

This paper investigates the dynamic response (mode shapes, resonance frequencies, and stress wave propagation) of moldable large-scale kerf panels with varying cut densities and

arrangements and the implications of reconfiguring kerf panels on their dynamic responses. The kerf panels consist of hexagon domains of triangular kerf patterns. The beam element model from Shahid et al. [12] is used to model the cells in the kerf structures. The kerf panels are cut from medium density fiberboard (MDF) which is modeled as a linear viscoelastic material. We first study the effect of two kerf parameters, i.e. kerf cut density and unit cell size, on the unit-cell modal behaviors. The response from the beam element model is validated using scanning laser vibrometry experiments on unit cells with different kerf densities. With an understanding of the effect of unit-cell density and size on the cell deformation and dynamics behaviors, large-scale kerf panels are designed and their corresponding dynamics responses are studied. Two kerf panels are considered, i.e., uniform cut density kerf panel and transitioning cut density kerf panel. The uniform cut density kerf panel is made up of hexagon cells of uniform cell size and cut density across the panel, whereas, the transitioning kerf panel is made up of a hexagon unit cell of uniform size with kerf cut density gradually varying across the kerf panel. The modal response of these kerf panels from the beam element model is validated using scanning vibrometer experiments. Moreover, we studied the effect of both local and global shape reconfiguration of kerf panels on their dynamic response. We also present the stress wave propagation of the reconfigurable kerf panels when exposed to dynamic loading.

The article is organized as follows. The beam element model is discussed in **Section 2** and **Section 3** explains the kerf patterns being studied. **Section 4** presents the modal response of kerf unit cells based on the kerf cut density and unit cell size. **Section 5** discusses the moldability of kerf panels and their corresponding dynamics response in terms of modal response, followed by the dynamic response (modal behavior and stress wave propagation) of reconfigurable kerf panels in **Section 6**. **Section 7** discusses the conclusions of this study.

## 2. Modeling of kerf structures using beam element model

To study the dynamics response of kerf structures, we use a beam element with a rectangular cross-section, which can undergo bending, axial stretching, transverse shearing, and twisting (see **Fig. 2**). The in-plane and out-of-plane large deformations in the beam elements are due to rotations while the axial stretch remains small compared to lateral deflections.

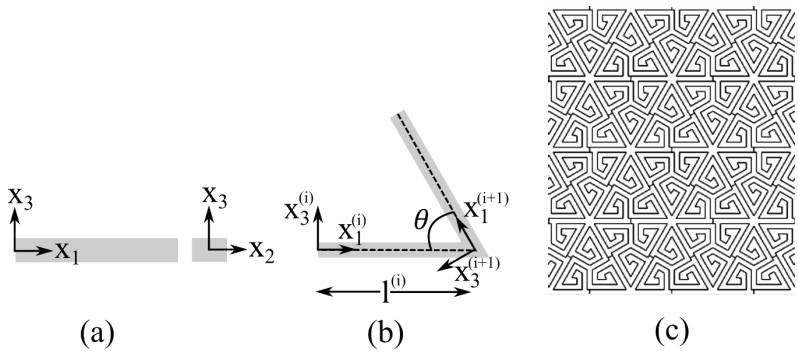


**Fig 2. Modeling kerf panels: a. Kinematic representation of continuous three-dimensional beam; b. Folded beam at θ=60°; c. Kerf structure**

The beam considered in this study can undergo both normal and shear strains (see **Fig. 2(a)**). The deformation in the straight continuous beam is given as:

$$\epsilon_{11} = \frac{du_1}{dx_1}(x_1,t) + x_3\frac{\partial\varphi_2}{\partial x_1}(x_1,t) - x_2\frac{\partial\varphi_3}{\partial x_1}(x_1,t) + \omega(x_2,x_3)\frac{d^2\beta}{dx_1^2}$$

$$\gamma_{12} = -\varphi_3 + \frac{\partial u_2}{\partial x_1} + \left(\frac{\partial\omega}{\partial x_2} - x_3\right)\frac{\partial\beta}{\partial x_1} \qquad \gamma_{13} = \varphi_2 + \frac{\partial u_3}{\partial x_1} + \left(\frac{\partial\omega}{\partial x_3} + x_2\right)\frac{\partial\beta}{\partial x_1} \tag{1}$$

where $\epsilon_{11}$ and $u_1$ are the strain and displacement in the axial direction, respectively, $\gamma_{12}$ and $\gamma_{13}$ are the transverse shear strains, $u_2$ and $u_3$ are the lateral displacements along $x_2$ and $x_3$ axes, respectively, $\varphi_2$ and $\varphi_3$ are the rotations due to bending about $x_2$ and $x_3$ axes, respectively, $\omega$ is the warping function, and $\beta$ is the angle of twist. As the MDF shows a viscoelastic response, it is modeled as an isotropic viscoelastic material in this study [27]. The equations of motion for the beam made up of MDF is summarized below:

$$AE * d\left(\frac{d^2u_1}{dx_1^2}\right) = \rho A\ddot{u}_1$$

$$kAG * d\left(-\frac{d\varphi_3}{dx_1} + \frac{d^2u_2}{dx_1^2}\right) = \rho A\ddot{u}_2$$

$$kAG * d\left(\frac{d\varphi_2}{dx_1} + \frac{d^2u_3}{dx_1^2}\right) = \rho A\ddot{u}_3$$

$$-I_{22}E * d\left(\frac{d^2\varphi_2}{dx_1^2}\right) - kAG * d\left(\varphi_2 + \frac{du_3}{dx_1}\right) = \rho I_{22}\ddot{\varphi}_2$$

$$I_{33}E * d\left(\frac{d^2\varphi_3}{dx_1^2}\right) - kAG * d\left(-\varphi_3 + \frac{du_2}{dx_1}\right) = \rho I_{33}\ddot{\varphi}_3$$

$$JG * d\left(\frac{d^2\beta}{dx_1^2}\right) = \rho I_p\ddot{\beta} \tag{2}$$

where $\rho$ is the mass density of the material, $A$ is the cross-sectional area, $I_{22}$ and $I_{33}$ are the second moments of an area about $x_2$ and $x_3$ axes, respectively, $I_p$ is the polar moment of an area, and $J$ is the torsional constant. The correction factor, $k$ is used to enforce uniform shear stress and shear strain distributions. The convolution operator in Eq. (2) means $F * dG = F(t)G(0) + \int_0^t F(t-s)\frac{dG(s)}{ds}ds$. The relaxation modulus is given as $E(t) = E(\infty) + \Delta E(t)$. The shear relaxation modulus can be determined from the extensional relaxation modulus using this relation: $G(t) = \frac{E(t)}{2(1+\nu)}$. In this study, Poisson's ratio is assumed time-independent $\nu$. The storage and the loss extensional moduli are expressed in terms of the relaxation modulus as:

$$\begin{aligned} E'(\omega) &= E(0) + \int_o^\infty \frac{d\left(\Delta E(s)\right)}{ds}\cos\left(\omega s\right)ds \\ E''(\omega) &= -\int_o^\infty \frac{d\left(\Delta E(s)\right)}{ds}\sin\left(\omega s\right)ds \end{aligned} \tag{3}$$

The storage and loss shear moduli are expressed as $G'(\omega) = \frac{E'(\omega)}{2(1+\nu)}$; $G''(\omega) = \frac{E''(\omega)}{2(1+\nu)}$.

The system of equations presented earlier are separable in time and space, and the vibration is harmonic in time, so the deformation solutions $\mathbf{q} = [u_1, u_2, u_3, \varphi_2, \varphi_3, \beta]^T$ have the following forms:

$$q_i(x_1, t) = \phi_i(x_1) y_i(t) = \phi_i(x_1) e^{r_i t} \tag{4}$$

The equations formed after substituting **Equation (4)** to **Equation (2)**, and imposing boundary and initial conditions lead to the characteristic equations, which are solved numerically to determine the resonance frequencies and corresponding mode shapes. The beam element is used to study the motion of kerf panels consisting of several folded beams with an arbitrary subtended angle, $\theta$ (see **Fig. 2(b)**) (discussed in **Appendix A**) [12]. As discussed in our previous study [12] the responses from the beam and continuum elements agree well in capturing the mode shapes and frequencies of kerf cells, while the beam element is computationally cost-effective when compared to the three-dimensional continuum element.

## 3. Kerf patterns

The kerf patterns considered are of a hexagon domain with a triangular spiral pattern, see **Fig. 3** [6, 9, 10], which are laser cut from an MDF board with a thickness ($t$) of 0.125 in. During laser cutting, the kerf gap width is kept at 0.015 in. There are various factors such as kerf gap width, kerf pattern, kerf cut density and size of the unit cell, etc. that affect the flexibility, load-bearing capacity, and dynamics response of the kerf structures [11]. In this study, we focus on two factors, i.e., kerf cut density and size of the unit cell by keeping the other factors constant. We consider unit cells (side length = 1 in.) cut with a triangular spiral pattern but different kerf cut densities. These kerf densities are referred to as HD (high density), MD (medium density), and LD (low density) as shown in **Fig. 3**. The HD unit cell has the highest number of cutlines with an edge length of the unit cell (1 in.) to width ($w$) ratio of 22. Whereas the MD unit cell has a relatively smaller number of cutlines compared to the HD unit cell with an edge length

of the unit cell (1 in.) to width ($w$) ratio of 16. The LD unit cell has the least number of cutlines with the edge length of the unit cell (1 in.) to width ($w$) ratio of 10. Therefore, the segments in the HD unit cell are relatively slenderer, have a lower second moment and polar moment, and lower torsional rigidity compared to MD and LD unit cell segments, which results in higher flexibility.

As mentioned earlier, the size of the unit cell can affect both modal response and frequency of the unit cell, so we considered four different sizes of kerf unit cells in this study, keeping the triangular cut pattern and number of cut lines the same for all the unit cells (see **Fig. 3**). All the unit cells are scaled with respect to the reference unit cell as shown in **Fig. 3**. In this study, the scaling factor is used to refer to different sizes of the unit cells. The scaling factor is calculated by the ratio of distances between two opposite corners of the respective hexagon and the reference unit cell. The ratio of width ($w$) to length ($l$) of the segments in the unit cell remains constant across different sizes of unit cells. Whereas, the thickness ($t$) of the segments, which is the thickness of the MDF board, is constant for all the sizes of the unit cell, which leads to decreasing ratio of the thickness ($t$) to length ($l$) of the segments as we go from the smaller to larger unit cell (see **Fig. 3**). The segments in the larger unit cells are slenderer compared to those of smaller unit cells, which makes larger unit cells overall more flexible. Due to relatively slenderer segments in the larger unit cells, we expect the modal response to show more out-of-plane mode shapes and lower resonance frequencies compared to smaller unit cells.

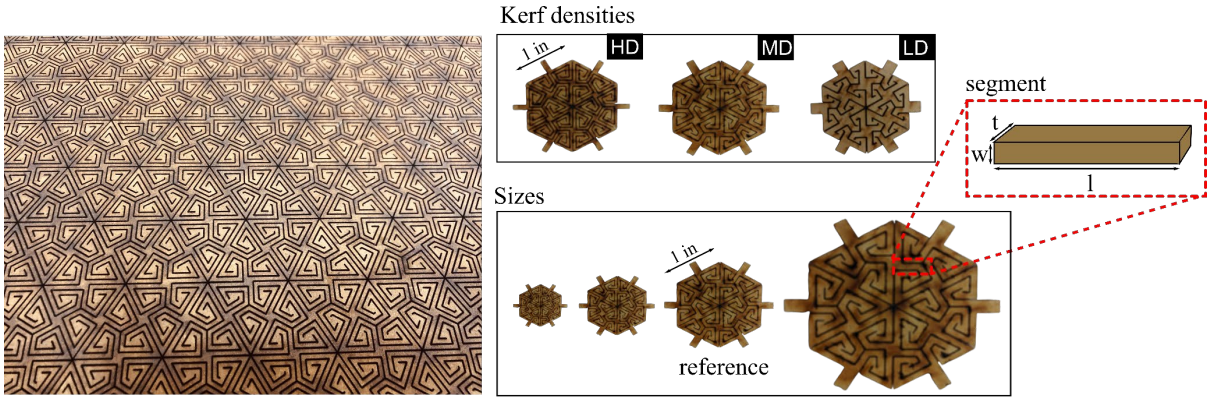


**Fig 3. Hexagon domain with triangular spiral pattern (left); unit-cells with different kerf densities (HD, MD, LD) and sizes (scaling factor: 0.5, 0.7, 1, 2) (right)**

## 4. Modal response of kerf unit cells

The segments in the unit cell were represented with beam elements of a solid cross-section. The mode shapes and modal frequencies depend on the geometric properties of the beams. For example, the HD unit cell has relatively slender beams so the beams mostly undergo in-plane bending ($x_1 - x_3$ plane), out-of-plane bending ($x_1 - x_2$ plane), and twisting (in-depth discussion in **Appendix B**). The LD region has relatively thick beams so they mostly undergo a combination of deformations such as axial stretching, transverse shearing, and out-of-plane bending. As the size of the unit cell is increased, the beams become slenderer which increases flexibility.

The clamped boundary conditions are imposed on the six handles of the kerf unit cell to simulate the unit-cell experiments. The relaxation modulus $E(t) = E(\infty) + \sum_{i=1}^{N} E_i e^{-t/\tau_i}$ of MDF is obtained from creep experiments on MDF dog-bone specimens [27]. The material parameters are given in **Table 1**.

**Table 1. Prony series parameters for MDF**

| $i$ | $\tau_i$ (s) | $E_i$ $(ksi)$ |
|---|---|---|
| 1 | 1000 | 96.3 |
| 2 | 3000 | 90.9 |
| 3 | 7000 | 87.4 |

### 4.1 Effect of kerf density on the modal response

All the unit cells (HD, MD, and LD) are generated using beam elements as shown in **Fig. 4**. Each beam in the unit cell has a thickness of 0.125 in., while the width of the beam depends on the kerf density. As the LD unit cell has a smaller number of cut lines compared to HD, the width of the beam element would be higher in the LD unit cell. The geometrical properties of the beam in each of the unit cells are shown in **Table 2**.

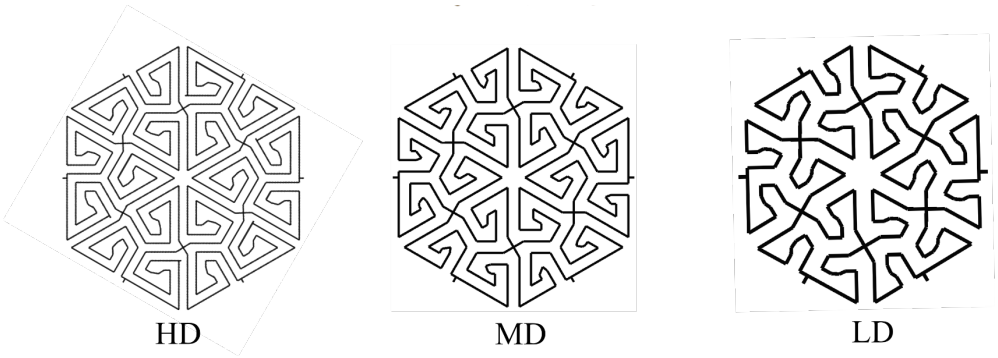


**Fig 4. Models for different kerf densities of unit-cells using beam elements**

**Table 2. Geometrical properties of beams in HD, MD, and LD**

| Unit cell | Area $(in^2)$ | Second Moment of area $I_{22}$ $(\times 10^{-5} in^4)$ | Second Moment of area $I_{33}$ $(\times 10^{-5} in^4)$ | Ratio of second moment of area $\frac{I_{22}}{I_{33}}$ | Torsional constant $J$ $(\times 10^{-5} in^4)$ | Ratio of second moment of area to torsion constant $\frac{I_{33}}{J}$ |
|---|---|---|---|---|---|---|
| HD | 0.125 × 0.0450 | 0.0949 | 0.7324 | 0.1296 | 1.1210 | 0.6533 |
| MD | 0.125 × 0.0633 | 0.2642 | 1.0303 | 0.2564 | 2.0160 | 0.5111 |
| LD | 0.125 × 0.1000 | 1.0417 | 1.6276 | 0.6400 | 4.8076 | 0.3385 |

To conduct modal experiments, custom-built fixtures are designed and fabricated to clamp the handles of the kerf unit cell specimens. The scanning laser vibrometry (PSV-500-3D, Polytec, Irvine, CA) is used to determine the modal response of these kerf unit cell specimens. More details about the experiments are given in [12].

The comparison of resonance frequencies and mode shapes from the model and experiment is shown in **Fig. 5** and **Fig. 6**, respectively. The model predicts the modal response of HD, MD, and LD unit cells. The LD unit cell, being the least flexible has the highest resonance frequencies compared to MD and HD unit cells. The low density of cut lines in the LD unit cell leads to higher width of the beam segments between the cut lines which increases the second moments and torsional constants, hence, making it stiffer as compared to HD and MD unit cells. The first mode of the LD, MD, and HD cells shows the same out-of-plane (dome-like) shape, which is governed by the flapping displacements (along $x_2$ axis) of the six triangular kerf cells. The higher modes are governed by the geometrical characteristics of the beam segments in the unit cells. The beam segments in the LD unit cell have a significantly higher ratio $\frac{I_{22}}{I_{33}}$ compared to beam segments in the MD and HD unit cell (see **Table 2**), making it easier for out-of-plane bending (along $x_2$ axis) than in-plane bending ($x_1 - x_3$ axis), and hence the out-of-plane bending dominates the response for the second and third modes of the LD unit-cell. Whereas the HD and MD unit cells have significantly low $\frac{I_{22}}{I_{33}}$ relative to the LD unit cell causes easier in-plane bending than out of plane bending. The beam element model can predict the modal response of the kerf unit cells. The kerf cut density influences the resonance frequencies and mode shapes of the kerf unit cells, which can have an impact on the dynamic response of kerf panels.

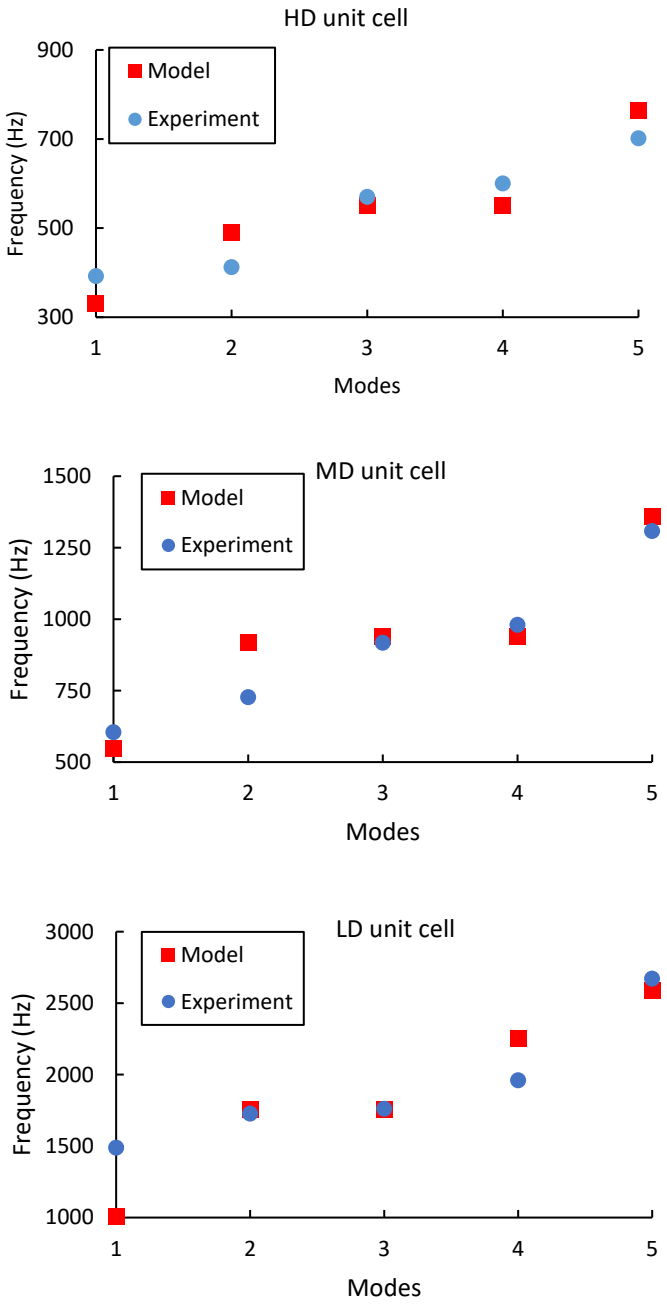


**Fig 5. Comparison of resonance frequencies for HD (RMSE (root mean square error): 58.15 Hz), MD (RMSE: 93.65 Hz), and LD (RMSE: 254.58 Hz) unit cell**

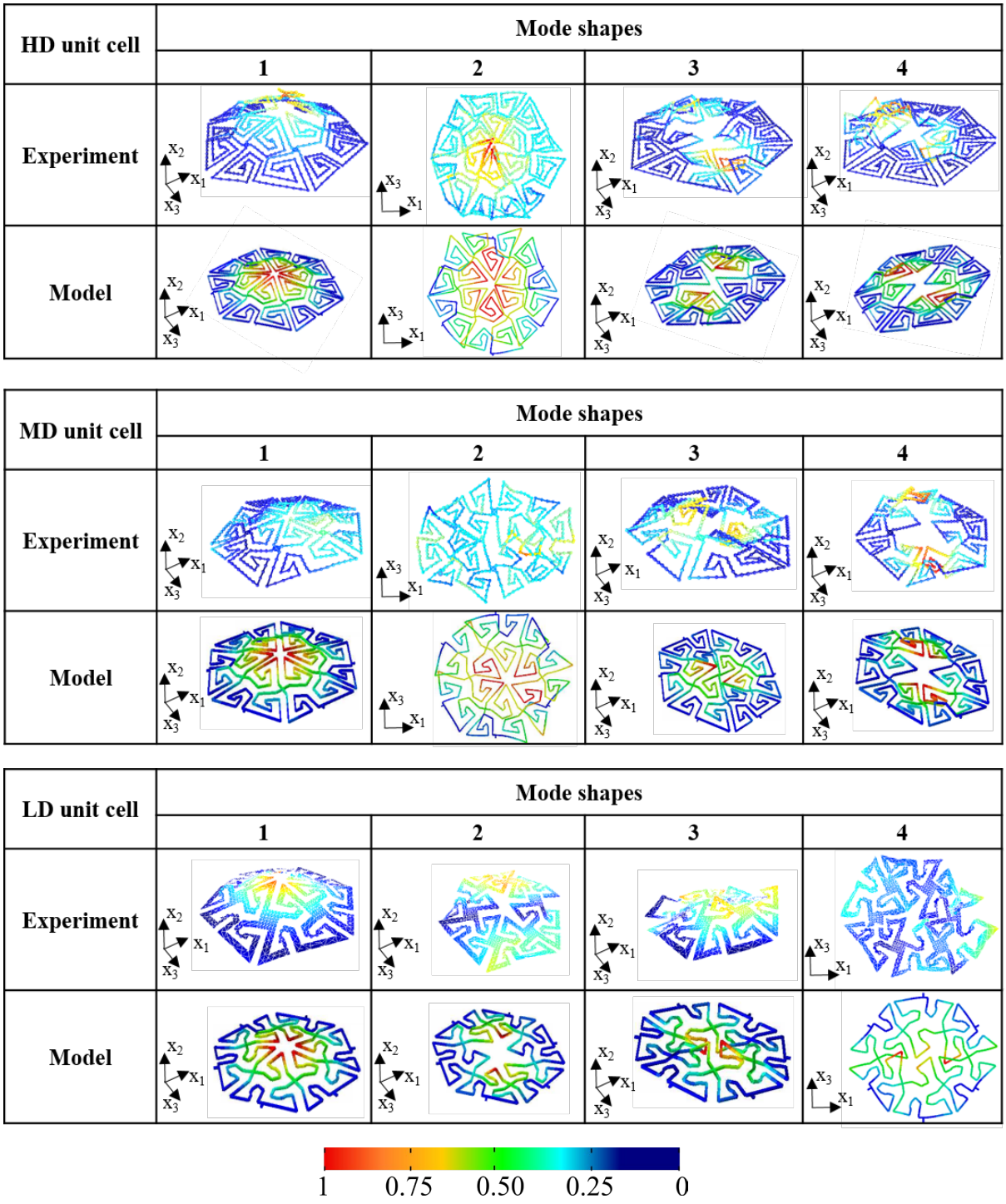


**Fig 6. Comparison of modal response showing normalized displacements for HD, MD, and LD unit cells**

### 4.2 Effect of unit-cell size on modal response

We examine the effect of the size of the unit cell on the dynamics of kerf unit cells using the beam element model. The beam element models of scaled unit cells are shown in **Fig. 7** and their geometrical properties of the beam in each of the unit cells are shown in **Table 3**. As mentioned earlier, the scaling factor is determined by taking the ratio of distance, $d$ for the respective unit cell and reference unit cell.

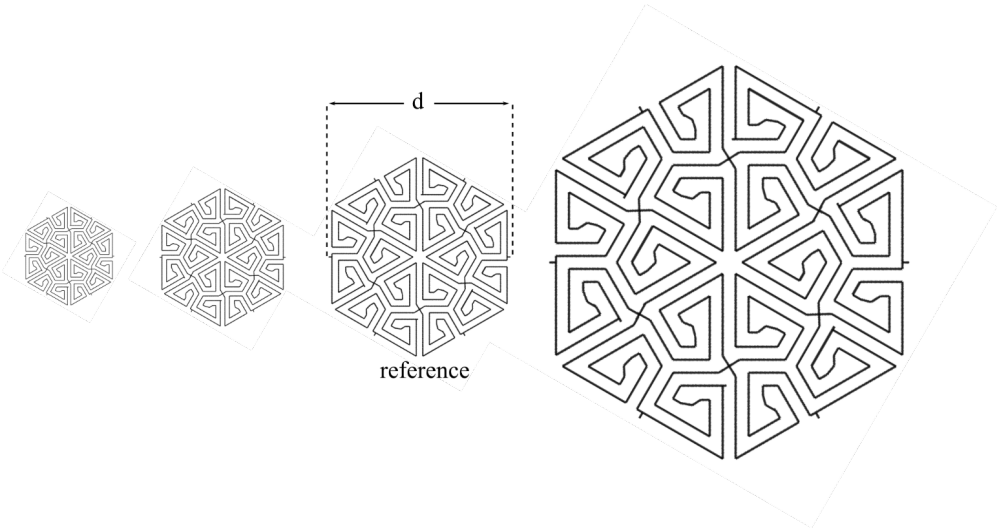


**Fig 7. Models for different sizes of unit-cells using beam elements; Scaling factor: 0.5, 0.7, 1, 2 (left to right)**

**Table 3. Geometrical properties of beams in different sizes of unit cells**

| Unit cell scaling factor | Area ($in^2$) | Second Moment of area $I_{22}$ ($\times 10^{-5} in^4$) | Second Moment of area $I_{33}$ ($\times 10^{-5} in^4$) | Ratio $\frac{I_{22}}{I_{33}}$ | Torsional constant $J$ ($\times 10^{-5} in^4$) | Ratio $\frac{I_{33}}{J}$ |
|---|---|---|---|---|---|---|
| 0.5 | 0.125 × 0.0225 | 0.0119 | 0.3662 | 0.0324 | 0.4202 | 0.8716 |
| 0.7 | 0.125 × 0.0315 | 0.0326 | 0.5127 | 0.0635 | 0.6548 | 0.7830 |
| 1 | 0.125 × 0.0450 | 0.0949 | 0.7324 | 0.1296 | 1.1210 | 0.6533 |
| 2 | 0.125 × 0.0900 | 0.7594 | 1.4648 | 0.5184 | 3.9148 | 0.3742 |

It is evident from the results shown in **Fig. 8** that the size of the unit cell influences the modal behavior of the kerf unit cells. The smaller unit cells are stiffer compared to large unit

cells as shown by their relatively high natural frequencies. The first mode in all sizes is out of plane (dome-like) shape, which is governed by the flapping displacements of the six triangular kerf cells. The beams in smaller unit cells are thicker, shorter in length, and have a lower ratio of $\frac{I_{22}}{I_{33}}$ compared to beams in larger unit cells (see **Table 3**). Therefore, smaller unit cells can undergo in-plane bending motion ($x_1 - x_3$ plane). In the largest unit cell, the out-of-plane bending ($x_1 - x_2$ plane) is easier to achieve as $\frac{I_{22}}{I_{33}}$ are significantly high compared to the smaller size of unit cells. The beams in large unit cells are slenderer relative to beams in small unit cells which contributes to flexibility and mode shapes showing out-of-pane motion. The beams in larger unit cells have higher torsional constant and lower $\frac{I_{33}}{J}$ compared to small unit cells so they undergo more out-of-plane bending relative to twisting as shown in **Table 3**. Additionally, different sizes of unit cells show paired modes. For example, 2$^{nd}$ mode in all the chosen sizes of unit cells has a paired mode shape but it is not shown. The paired mode shape is omitted to show higher mode shapes which helps understand the influence of kerf unit cell sizes on the dynamics behavior. The size of the unit cell can significantly influence the modal behaviors due to changes in the geometrical properties of the beam segments in the unit cells.

| Scale factor | Modes | | | | |
|---|---|---|---|---|---|
| | 1 | 2 | 3 | 4 | 5 |
| 0.5 | 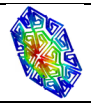 |  | 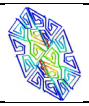 | 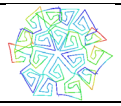 | 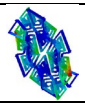 |
| | 752.32 Hz | 982.36 Hz | 1225.30 Hz | 1578.50 Hz | 1832.30 Hz |
| 0.7 | 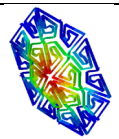 | 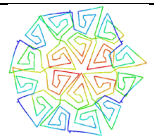 | 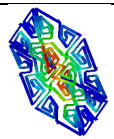 | 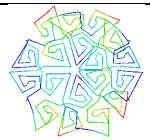 | 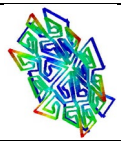 |
| | 512.69 Hz | 701.68 Hz | 840.61 Hz | 1127.50 Hz | 1275.50 Hz |
| 1 (reference) | 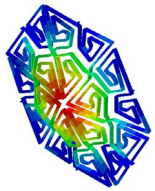 | 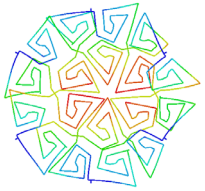 | 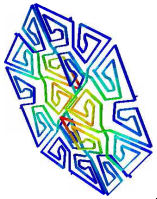 | 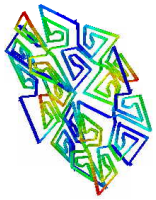 | 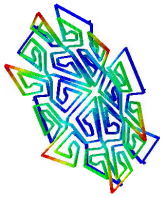 |
| | 331.25 Hz | 491.21 Hz | 549.54 Hz | 764.69 Hz | 844.22 Hz |
| 2 | 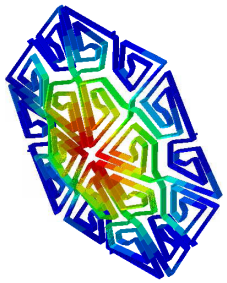 | 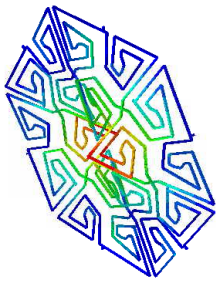 | 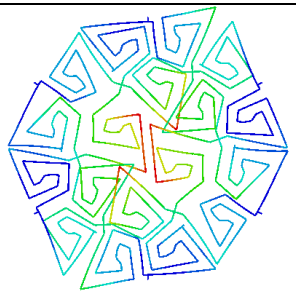 | 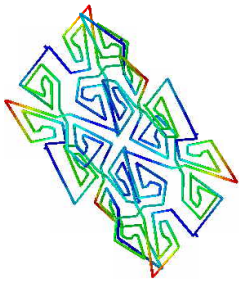 | 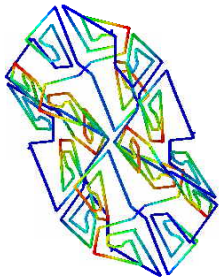 |
| | 123.46 Hz | 211.96 Hz | 260.76 Hz | 329.87 Hz | 360.79 Hz |

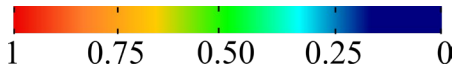


**Fig 8. Modal behavior showing normalized displacements for different sizes of kerf unit cells**

## 5. Moldability of Kerf Panels and their Modal Behaviors

Based on our understanding of the effect of the kerf densities and sizes on the modal response of the unit cell, we study the moldability of the kerf panels into freeform shapes and their corresponding dynamic response. The kerf panels in this study are cut from the MDF board have a side length of 17 in. and thickness of 0.125 in. The kerf panels are also modeled using the beam element model to analyze the deformed shapes and predict the modal behavior of kerf panels.

We consider a case study to create freeform shapes with multiple high gradients of local curvatures in the neighboring areas (see several examples in **Fig. 9**). Two different large-scale kerf panels (uniform density kerf panel and transitioning density kerf panel) are generated to demonstrate the idea of local flexibility, which can be obtained from varying kerf parameters of the unit cells. The uniform density kerf panel has a similar repeatable kerf pattern across the panel (see **Fig. 10**), whereas, the transitioning density kerf panel has varying kerf cut density across the panel (see **Fig. 11**).

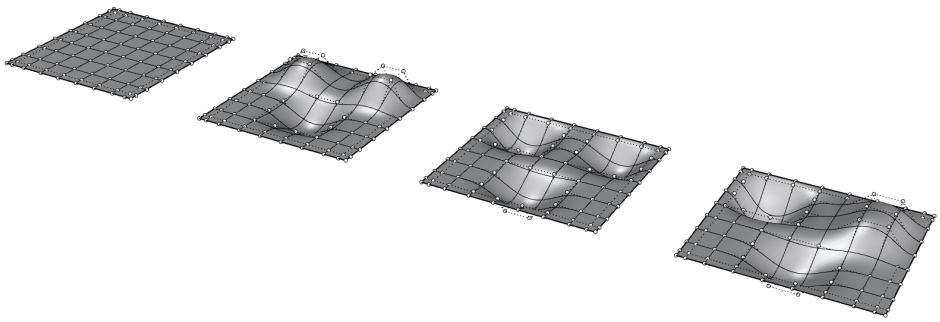

**Fig 9. Example of freeform macroscopic shapes with multiple high gradients of local curvatures**

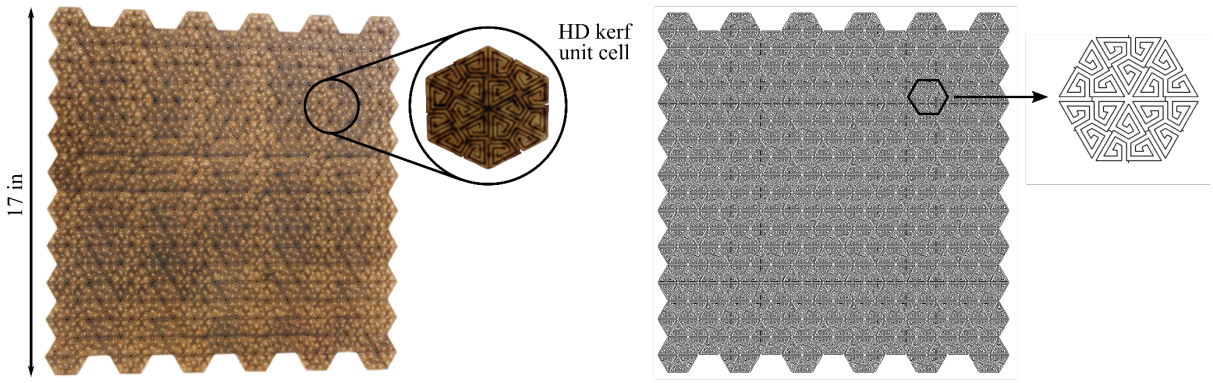


**Fig 10. Uniform kerf panel made up of HD kerf unit cells (left); Model for uniform kerf panel made using beam elements (right)**

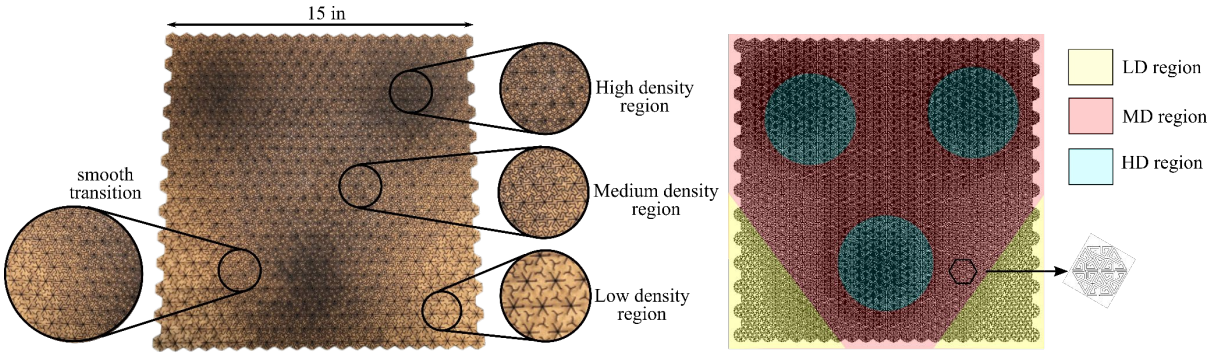


**Fig 11. Transitioning kerf panel (left); Model for transitioning kerf panel made up of small kerf unit cells (scaling factor: 0.7) using beam elements (right)**

The similar cut density across the panel in the uniform density kerf panel leads to uniform stiffness across the panel which inhibits local flexibility. Therefore, it becomes impossible for the uniform density kerf panel to be molded into a shape with multiple high curvature regions in proximity with a minimal actuation, i.e., three contact points of deformation. Instead, the uniform kerf panel shows a global out-of-plane shape with rather indistinguishable high local curvatures as shown in **Fig. 12 (top)**. By varying cut density across the transitioning kerf panel, the stiffness varies across the panel and more complex shapes can

be easily achieved. This leads to greater local flexibility in regions with a high density of cutlines relative to other regions in the panels. Thus, the transitioning kerf density panel can be molded into complex freeform shapes with multiple local curvatures with minimal actuation (see **Fig. 12 (bottom)**). While the uniform kerf density kerf pattern can be molded into macroscopic shapes with low gradients of local curvatures.

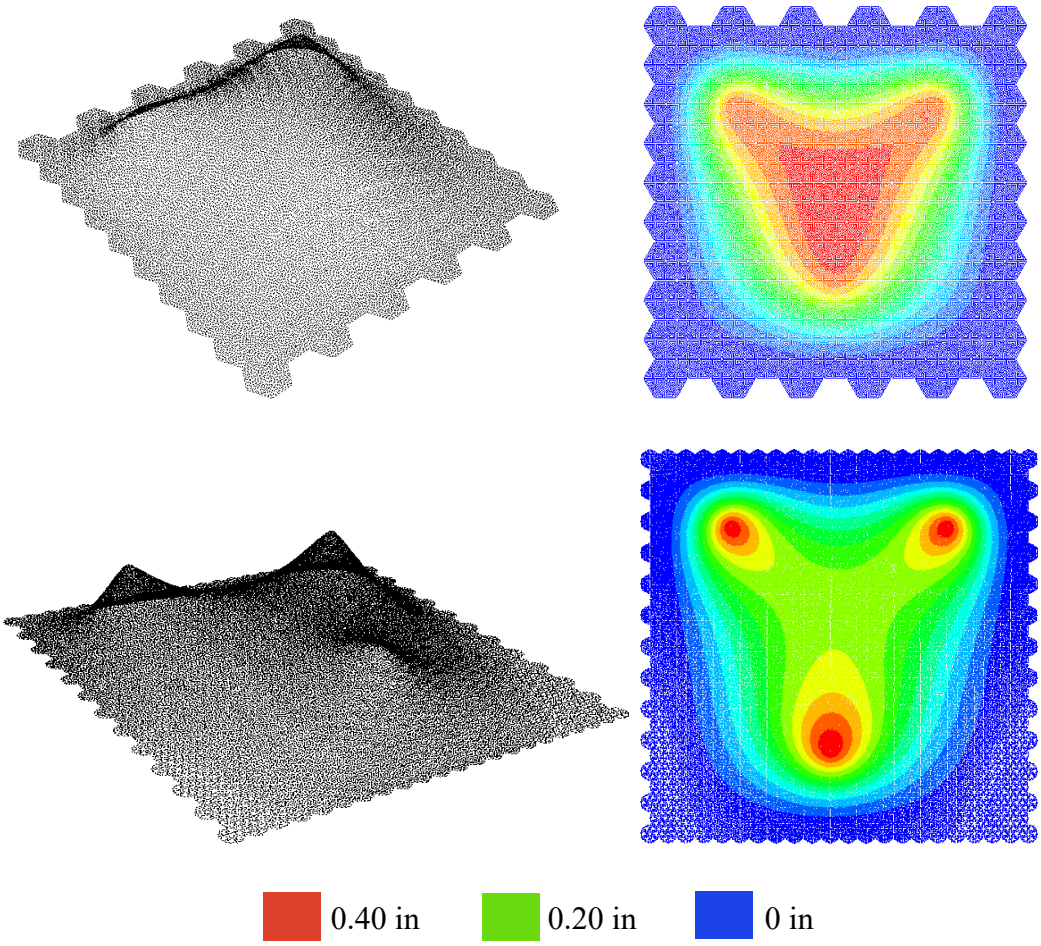


**Fig 12. Uniform (top) and transitioning (bottom) kerf panels can mold into complex macroscopic shapes (color contour defines out of plane displacements)**

### 5.1 Modal Response of Uniform Density Flat Kerf Panel

We first studied a kerf panel made up of uniform HD unit cells of size (scaling factor: 1) across the panel as shown in **Fig. 10**. To determine the modal response, the Lanczos method is used to determine the natural frequencies and modal response of the system [28]. The edges of the kerf panel are not constrained so free-free boundaries are implemented on the edges.

The experiments are also performed on the uniform kerf panel to validate the mode shapes and corresponding modal frequencies determined from the beam model. The experimental details are discussed in **Appendix C**. The comparison of modal behavior is shown in **Fig. 13**. The beam element model simulation can capture the modal response determined from the experimental tests. However, there are discrepancies in the model predictions and experimental results in the higher modes (>11) which are discussed in **Appendix C**. The lower order mode shapes are governed by global modes of plates, which are out of plane ($x_1 - x_2$ plane) mode shapes. Local in-plane and out-of-plane deformations in the individual cells are much more difficult to obtain. When unit cells are combined to form a panel, the ratio of overall length to thickness (slenderness ratio) of the panel increases compared to a single unit cell. The high slenderness ratio of the kerf panel compared to a single unit cell leads to an out-of-plane motion being dominant in the earlier modes. Whereas, in-plane ($x_1 - x_3$ plane) mode shapes (local displacements of the individual cells) are observed after the 35$^{th}$ mode in which the beams of the panels undergo bending about $x_2$ axis as determined from the beam element model.

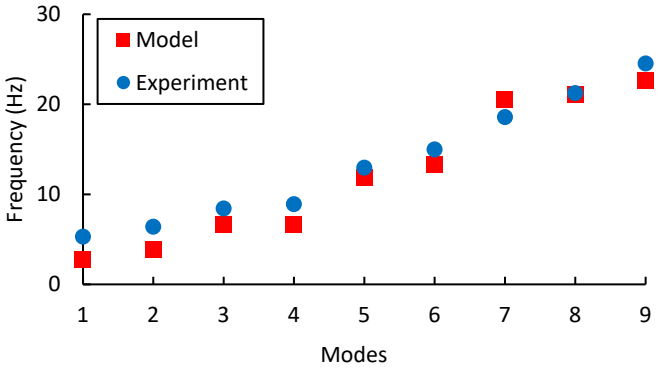


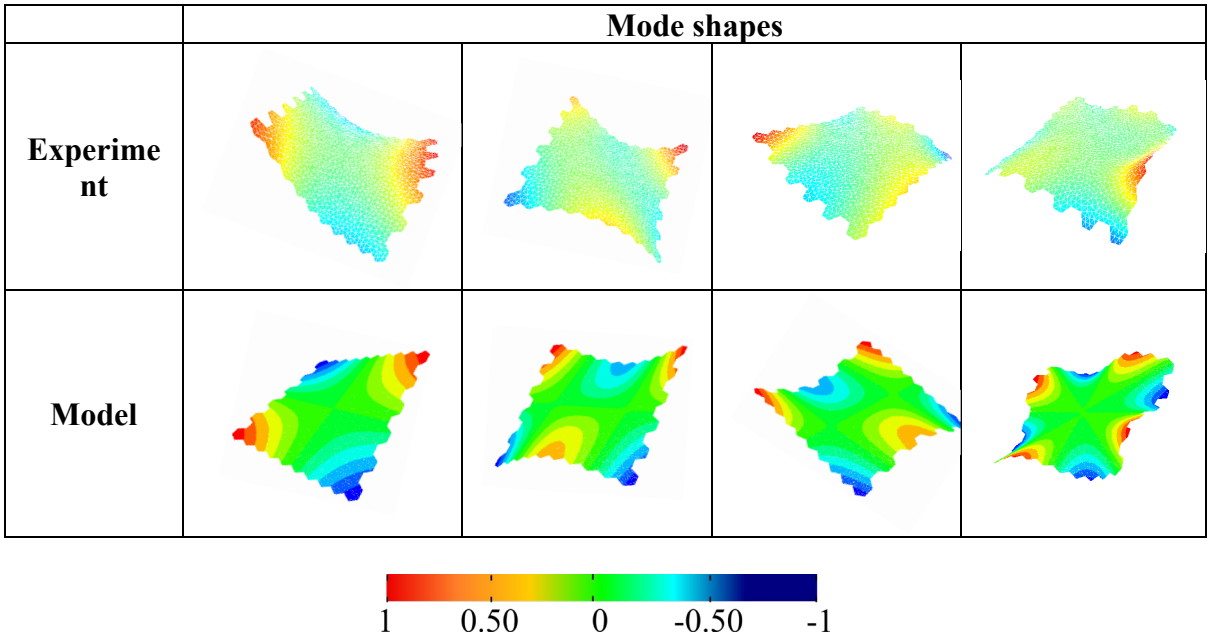


**Fig 13. Comparison of modal response showing normalized out-of-plane displacement for uniform kerf panel (RMSE: 1.97 Hz)**

### 5.2 Modal Response of Transitioning Density Flat Kerf Panel

We now explore the influence of variable kerf densities and the size of the unit cells on the dynamic response of the kerf panels. Unlike the uniform kerf density panel, the transitioning kerf density panel has a gradually varying kerf density (see **Fig. 11**). The size of the unit cell (scaling factor: 0.7) is smaller compared to the reference unit cell in the uniform kerf panel.

The density of the cut lines is varying gradually over the surface which leads to a variable cross-section of the beams in the transitioning kerf panel. We used the average cross-

section of the beams in different regions of the transitioning kerf panel. The region in blue is modeled with high density (HD), a region in red is modeled with medium density (MD), and the region in yellow is modeled with low density (LD) (see **Fig. 11**). Each beam has a thickness of 0.125 in. and the width of the beam depends on the kerf density and size of the unit cell.

The modal response from the beam element model and experiments is determined similarly as it was done for the uniform kerf panel. More details specifically about the experimental method for the transitioning kerf pattern are discussed in **Appendix C**. Overall, the modal response from the simulation and experiment match very well except for greater disagreements in the higher-order modes (>11) (see **Appendix C** for an in-depth discussion). From **Fig. 14** it is seen the transitioning kerf panel shows different mode shapes compared to the uniform kerf panels. By varying the kerf density across the panel, paired modes are not observed in the modal analysis. In the transitioning panel, the HD cut region is more compliant relative to LD and MD cut region [29]. Whereas in the LD and MD cut regions, the beams have a higher second moment and torsional constants compared to the HD region, which restricts bending and twisting in these regions. Due to the MD and LD cut region in the transitioning kerf panel, the transitioning kerf panel has higher modal frequencies compared to the uniform kerf panel (see **Fig. 13** and **Fig. 14**). The contrast of different kerf densities in the transitioning kerf panel leads to a variety of deformation behaviors across the panel. For example, the LD cut regions at the bottom of transitioning kerf panel in earlier mode shapes undergo less bending due to high second moment of area, $I_{33}$ relative to other cut regions in the panel. In addition to different kerf densities in the panel, the small size (scaling factor: 0.7) of the unit cell also influences the modal frequency of the transitioning kerf panel. As mentioned earlier the smaller unit cells are stiffer relative to large unit cells, this also leads to higher stiffness of transitioning panel compared to uniform kerf panel.

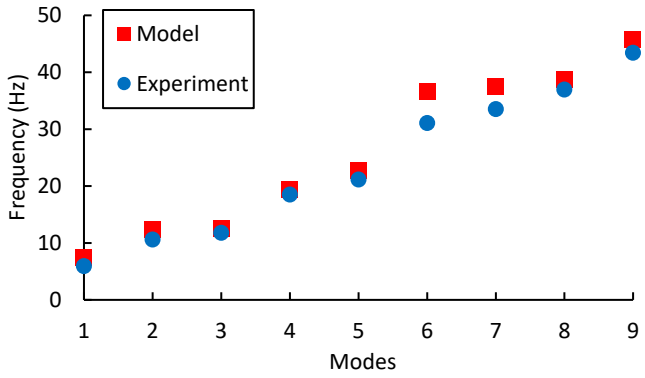


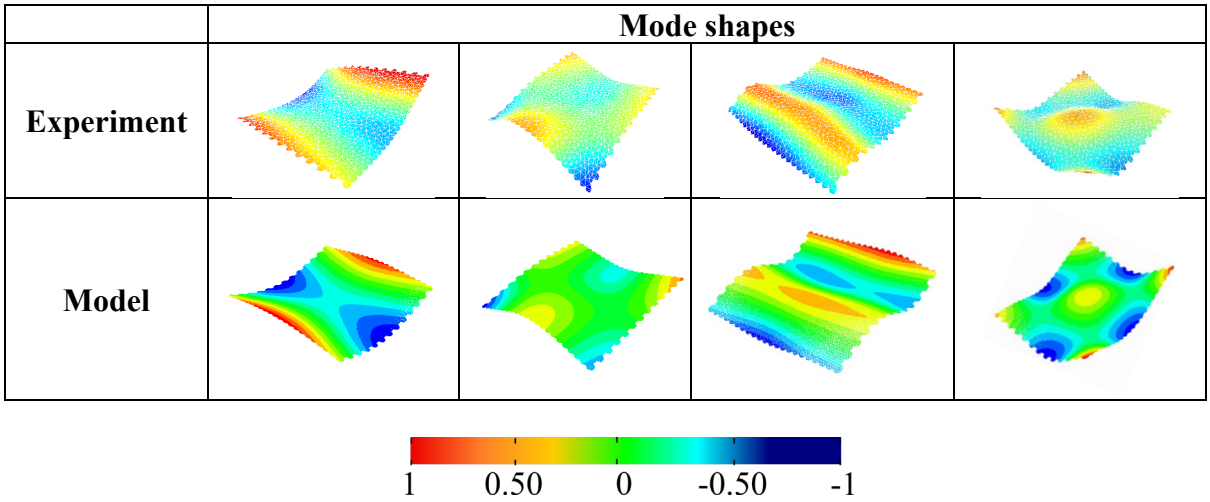


**Fig 14. Comparison of modal response showing normalized out-of-plane displacement for transitioning kerf panel (RMSE: 2.68 Hz)**

Overall, the analysis on large-scale kerf panels demonstrated the capability of the beam element model to capture the modal response of kerf panels. Modal response of large-scale kerf structures can be altered by varying kerf density and size of the unit cell.

## 6. Dynamics Analyses of Freeform Kerf Panels

The idea of using kerf panels is to achieve freeform shapes, and at the same time, the kerf cells can be easily deformed to alter the dynamics response of the structures. We study the dynamics behavior of the kerf panels that are molded into different shapes. Global reconfigurations of the kerf panel can induce pronounced stresses in the multiple unit cells, which significantly influences the panel dynamic behavior. Conversely, local perturbation of the kerf panel can

induce stresses in a small region of a unit cell which has an insignificant effect on the dynamic behavior of the panels (see **Appendix D**). The stresses due to shaping the kerf panels are taken into consideration when determining the modal behavior of freeform kerf panels.

### 6.1 Modal Analyses of Moldable Kerf Panels into Freeform Shapes

We first explore the dynamics response of a uniform kerf panel with clamped edges. We shaped the panel into a dome shape by inducing an out-of-plane displacement of 1 in. at the center, as shown in **Fig. 15**. We also presented an analysis on tuning the dynamic response of a flat kerf panel by inducing a small out-of-plane displacement of 0.04 in at a small segment of one triangular unit cell at the center (see **Fig. 15**), which we refer to as a local perturbation. This analysis is run in two steps. In the first step, the kerf panel is deformed into the corresponding shape by applying a displacement loading. Whereas, in the second step, modal analysis is run on the shaped kerf panel. During the modal analysis step, all nodes in the shaped kerf panel are free to move to study the effect of shape reconfiguration on the modal behavior accurately.

With a dome shape in the uniform kerf panel, the modal response of the kerf panel is considerably altered from the corresponding flat kerf panel as shown in **Fig. 15**. The shape of the dome kerf panel remains symmetric, so the corresponding mode shapes show symmetric or antisymmetric shapes, and paired modes are also observed. The dome-shaped kerf panel is stiffer compared to a flat panel as shown by relatively higher resonance frequencies. The mode shapes and frequencies of the flat kerf panel involved in the dome shape deformation experience the highest changes. For example, mode 1 of flat uniform kerf panel experiences the highest rise in the modal frequencies and we no longer see a dome-like mode shape in the dome-shaped kerf structures (see **Fig. 15**). Thus, we can alter certain mode shapes in the flat kerf panel by inducing proper shape changes to the kerf panel. The flexibility of kerf panels enables easy shape reconfigurations.

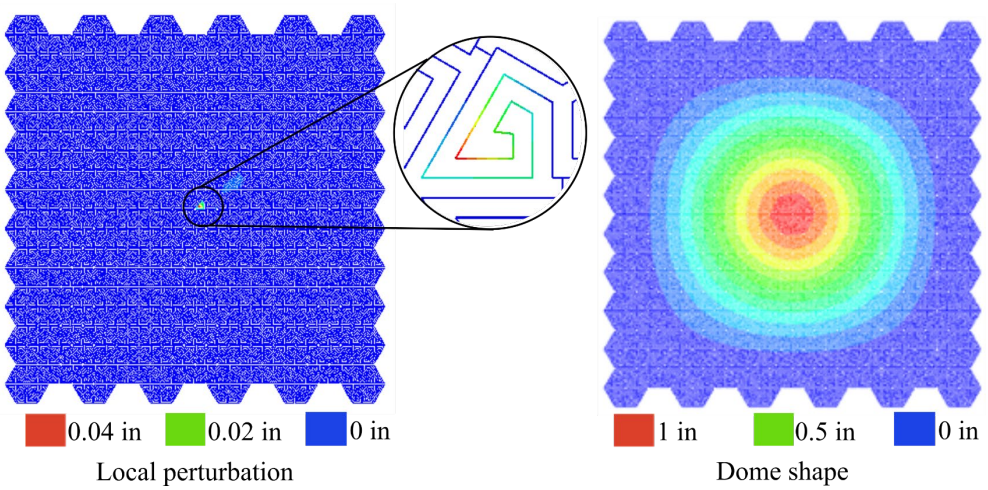


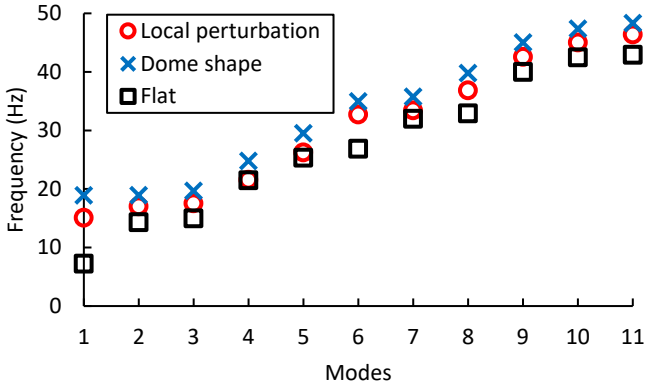


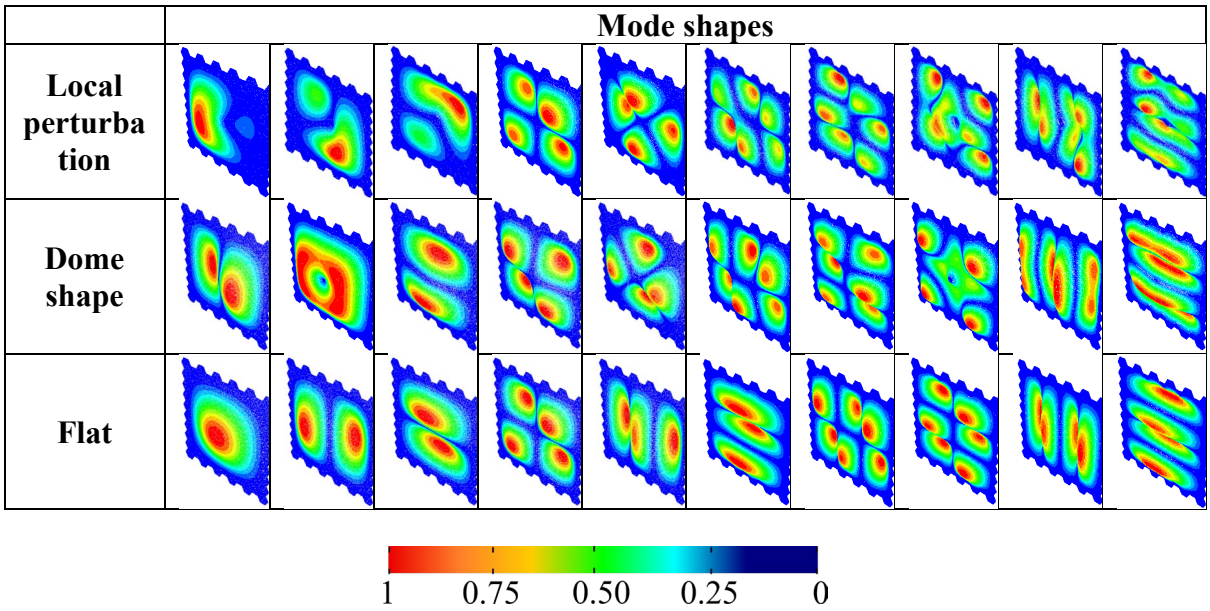


**Fig 15. Uniform density kerf panel microscopically and macroscopically deformed (top); Modal frequency comparison (middle); Mode shape comparison showing normalized displacements (bottom)**

Additionally, by only marginally varying the local shape of the kerf panel, the modal response can be significantly altered. The local perturbation as shown in **Fig. 15** breaks the symmetric mode shapes and eliminates paired modes. Even with a small local perturbation in the panel, several mode shapes of the flat panel can be avoided. During the local perturbation, only one region of a triangular unit cell is deformed, so the resonance frequencies of the locally perturbed kerf panel are less affected, except for the ones that are directly involved with the local perturbation deformation, e.g., modes 1 and 6.

Similar studies are also performed on a transitioning density kerf panel. The transitioning density kerf panel can be easily actuated to achieve high curvature regions in neighboring areas as previously shown in **Fig. 10**. To achieve the multiple high curvature shape change, the edges of the transitioning density kerf panel are clamped and three high density cut regions in the panel are actuated with an out-of-plane by 0.4 in. as shown in **Fig. 16**. We also consider local perturbation in the transitioning density kerf panel by actuating three triangular unit cells in three high dense regions by 0.04 in. as shown in **Fig. 16**.

With multiple high curvatures in the kerf panel, the modal response is significantly altered compared to the flat panel. The deformed panel is stiffer compared to the flat kerf panel as shown by higher resonance frequencies. Although both deformed and flat kerf panels show out-of-plane mode shapes, there is a substantial difference in the mode shapes. The mode shapes of the multiple high curvature deformed panel only show out-of-plane motion around the high curvature regions. In the local perturbation, only small regions i.e. three triangular unit cells of hexagon domains undergo stresses, which leads to less change in resonance frequencies compared to the multiple high curvature deformed panel. The mode shapes for the locally perturbed kerf panel are however altered considerably compared to the flat kerf panel. This once again shows that kerf panels enable easy manipulation of dynamics response of the structures by macroscopic shape changes and/or local perturbation.

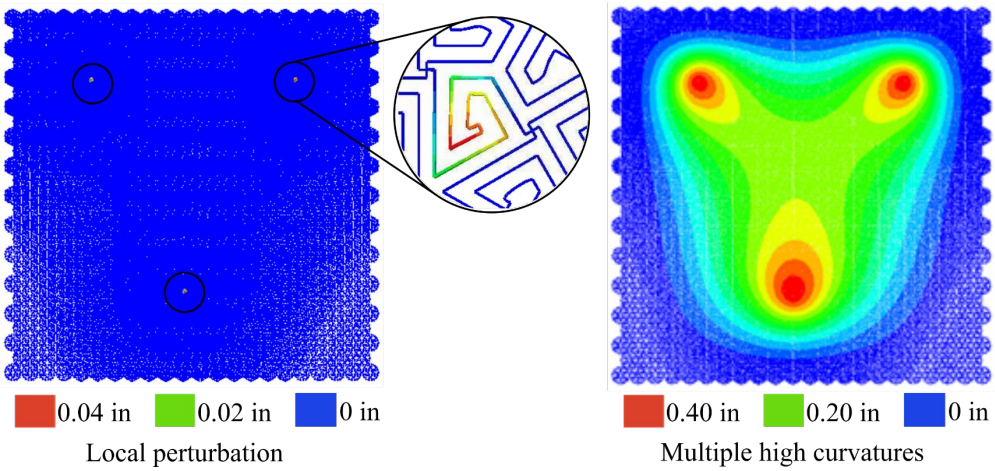


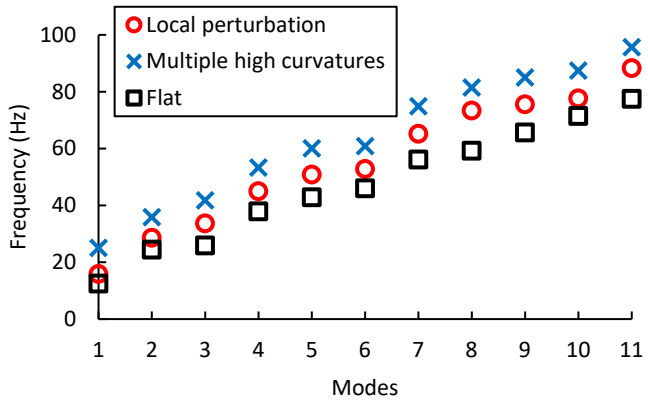


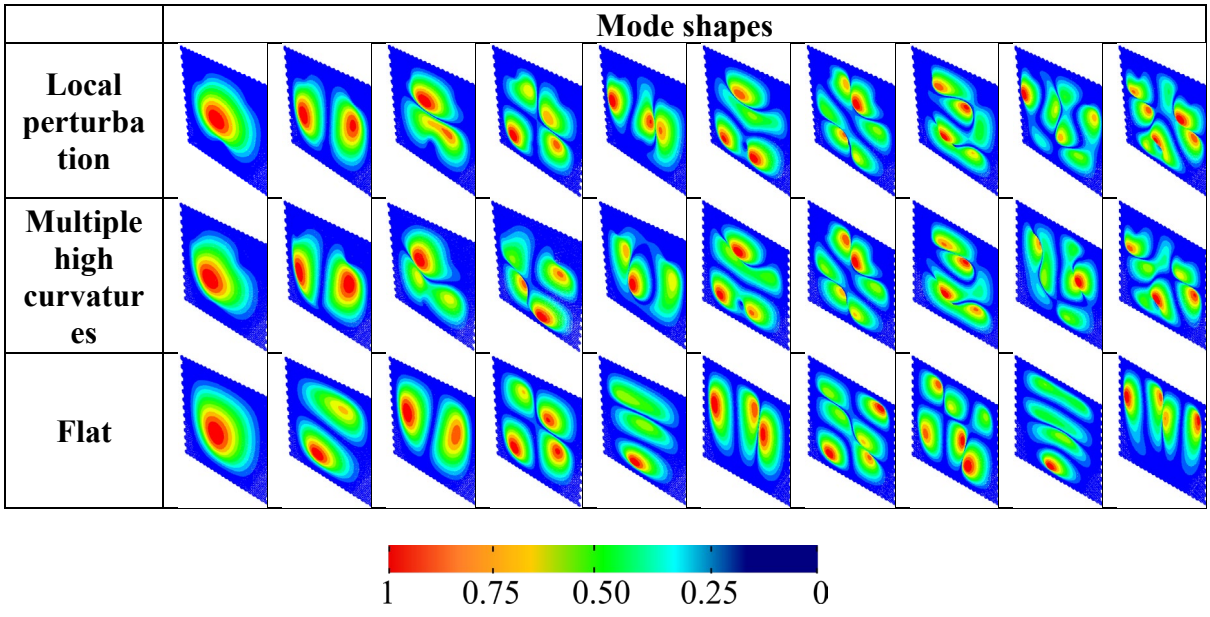


**Fig 16. Deformed transitioning kerf panel and displacement contour (top); Modal frequency comparison (middle); Mode shape comparison showing normalized displacements (bottom)**

It can be concluded that by reconfiguring the kerf panels into different macroscopic and/or microscopic shapes we can alter the resonance frequencies and mode shapes. This merit of large-scale kerf panels is useful for structural applications exposed to dynamics loading, i.e. avoiding resonance in building facades, mitigating vibrations in morphing structures, etc.

### 6.2 Wave Propagation in Reconfigurable Kerf Panels

We now examine the stress propagation behavior of large-scale kerf structures. We first determine the stress wave propagation in flat kerf panels cut with uniform and transitioning cut densities. The stress wave propagation in these kerf panels is compared against a flat solid panel. The panels are clamped at the edges and perturbed with an impact force at the center as

$$f(t) = \begin{cases} f_o\left(1 - \frac{t}{t_s}\right) & 0 \le t \le t_s \\ 0 & t < 0 \; and \; t > t_s \end{cases} \quad (5)$$

where $f_o = 1lb_f$ and $t_s = 0.005s = 5ms$. From the analysis, we calculated von Mises stress at two locations, i.e., in the center and on the left corner as shown in **Fig. 17** and **Fig. 18**. In addition to this, we determined stress decay percentage ($\frac{\sigma_t}{\sigma_{max}} \times 100\%$) at the center and the left corner as shown in **Fig. 19**, where $\sigma_t$ is the von Mises stress magnitude at a time, $t$ and $\sigma_{max}$ is the maximum von Mises stress magnitude experienced by the panel during the impact. The scale of the ordinate axis is limited to 50% to better compare the stress decay in the panels.

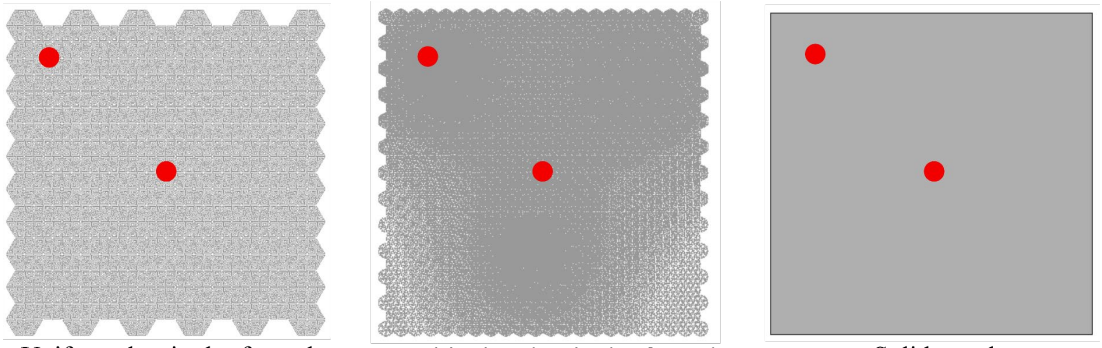


**Fig 17. Stresses determined at two locations; center and top left corner**

During excitation, the stress wave propagates from the center towards the edges. As solid panel does not have any gaps, the stress propagates faster towards the edges compared to kerf panels [12]. When the loading is stopped, the kerf panels retain stress and keep vibrating due to their flexible nature for a relatively long time compared to the solid panel as shown in **Fig. 18**. Due to a concentrated loading at the center, the center region of the kerf panels undergoes high localized out-of-plane deformation which leads to overall higher stress amplitudes in the kerf panels compared to the solid panel. Among all the panels, the uniform density kerf panel experiences the highest von Mises stresses at the center of 2000 psi. This stress is sufficiently lower than the tensile strength of MDF (3500 psi). The ordinate axis scale in **Fig. 18** is shown only up to 1000 psi to better compare the stress-time history in all the panels.

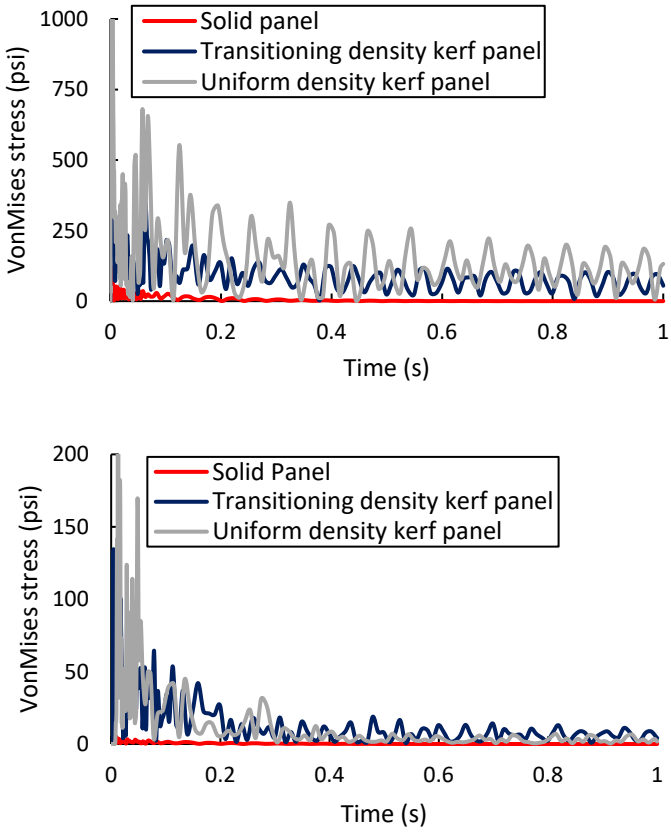


**Fig 18. Comparison of stress wave propagation (Von Mises stress) in flat kerf panels and flat solid panel at the center (top) and top left corner (bottom)**

The kerf cut density affects the stress propagation response of the kerf panels. The stress decay is approximately similar at the center in both uniform and transitioning kerf panels (see **Fig. 19 (top)**). However, away from the impacted region at the corner, the uniform density kerf panel not only slows down wave propagation but also leads to a more significant decay in stress magnitude compared to transitioning kerf panel (see **Fig. 19 (bottom)**). In the corner, the decay in stress in the uniform density kerf panel is similar to the one in the solid panel (seem to cease after 0.3 sec) (see **Fig. 19 (bottom)**). The uniform kerf panel is more flexible compared to the transitioning panel (see a discussion in **Section 5**) which causes easy vibrations around the impacted region and consumes most of the kinetic energy from the impact.

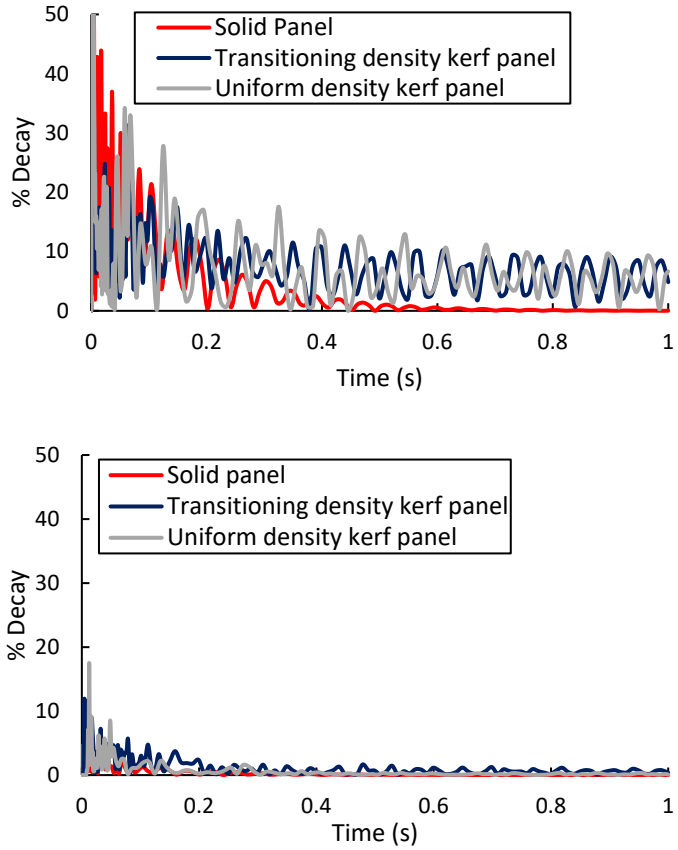


**Fig 19. Comparison of stress decay in flat kerf panels and flat solid panel at the center (top) and top left corner (bottom)**

The idea of cutting kerf panels with transitioning kerf patterns is to configure them into desired shapes as explained earlier. Reconfiguring kerf panels leads to a significant change in the modal behavior (resonance frequency and mode shapes) as shown in **Section 6.1**. Now, we further investigate how the shape change affects the stress wave propagation in the kerf panels. In this analysis, the transitioning kerf panel is clamped at the edges and deformed into a shape with multiple high curvatures as shown in **Fig. 16**. Subsequently, it is subjected to impact force load the center with the loading condition mentioned in **Equation (5)**, where $f_o = 1\ lb_f$ and $t_s = 0.005\ s$. For comparison, the MDF solid panels are also deformed into the shape with multiple high curvatures and subjected to similar loading conditions.

Due to the transitioning kerf pattern, the kerf panel can be easily reconfigured into a shape with multiple high curvatures. Whereas chopped MDF fibers and resin need to be processed in a mold with high curvatures to construct the desired deformed shapes out of a solid panel. The shape reconfiguration alters the stress propagation behavior of both solid and kerf panels. The deformed panels, both solid and kerf panels, can delay the propagation of the stress waves towards the edges compared to the flat panels (see **Fig. 20**). As the stress is being attenuated during the propagation, the delay in wave propagation can further reduce the amplitude of stress when it reached the edges. During force loading, the stress wave in the solid panel takes 0.7 ms to travel towards the edges compared to transitioning kerf panel, which takes 4.0 ms (see **Fig. 20**). It is seen that the flexible and compliant nature of the kerf panels makes it easy to reconfigure their shapes to alter the stress wave propagation behaviors. In this case, the reconfigured panels with multiple high curvatures slow down the wave propagation, leading to significantly reduced stress amplitude as the wave propagates.

We demonstrated that the geometrical patterns and shapes of kerf panels influence the stress wave propagations of MDF kerf panels. We further examine the effect of delayed responses of viscoelastic materials on the stress wave propagation in Appendix E.

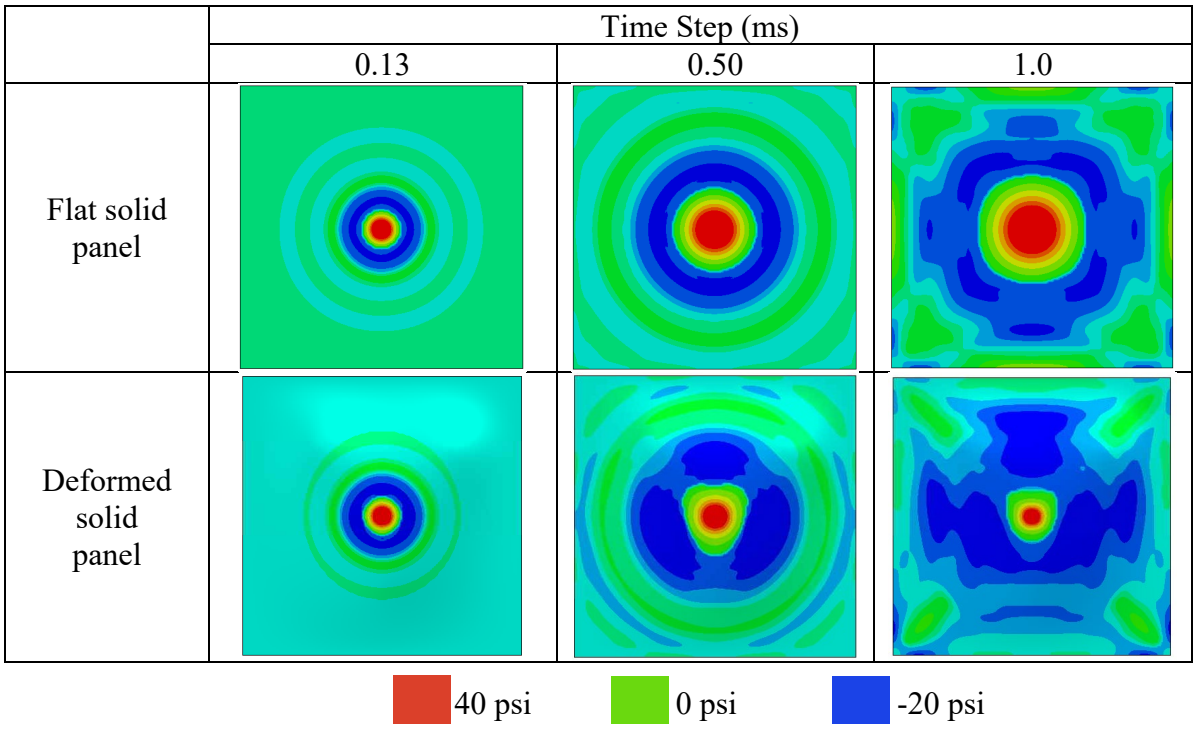


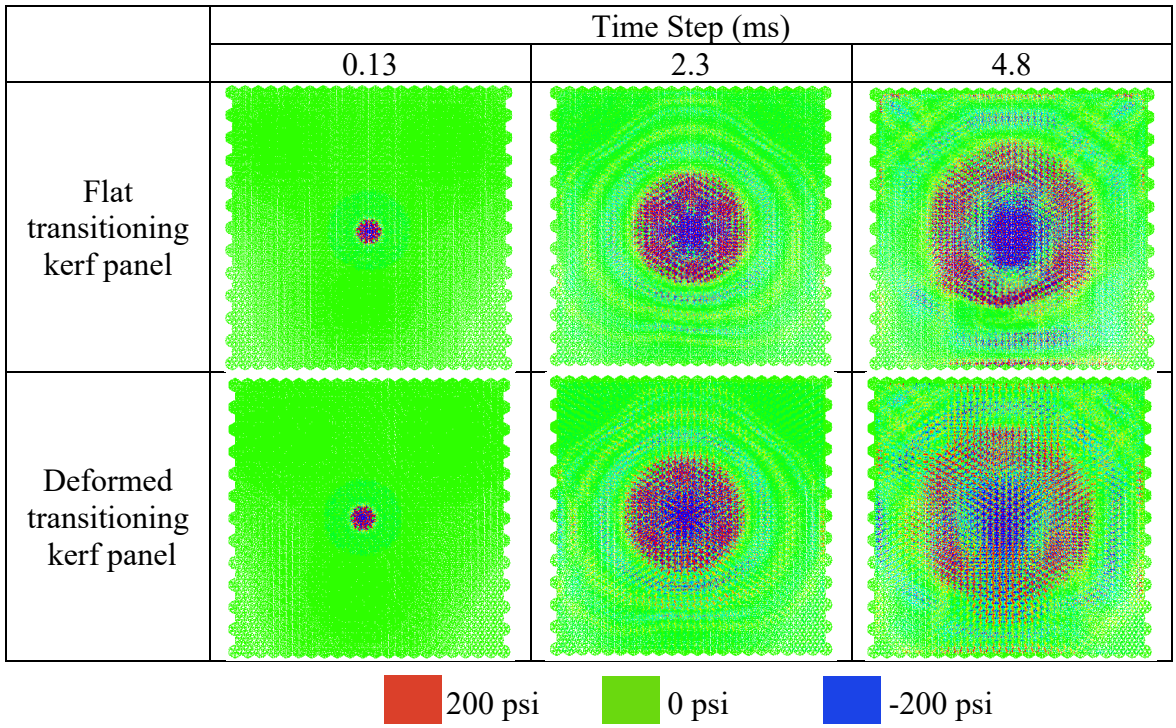


**Fig 20. Stress wave propagation (maximum principal stresses) in solid panel (top) and transitioning density kerf (bottom)**

## 7. Conclusion

This research focuses on studying the dynamic response of reconfigurable kerf structures in terms of mode shapes, modal frequencies, and stress wave propagation. We have investigated kerf unit cells of a hexagon domain out of MDF of a fixed thickness of 0.125 inches to understand the influence of kerf cut density and unit-cell sizes on the modal response of the kerf unit cells. Experimental tests using scanning laser vibrometry have been conducted and a mathematical model has been used to understand the modal response of the kerf unit cells. A beam element model with a viscoelastic material was used to describe the deformations of each segment in the kerf unit cell. We have shown that geometrical parameters, i.e. second moments of an area, torsional rigidity, and slenderness ratio, of the beam segments in the kerf unit-cell control the mode shapes and frequencies. Slenderer beam segments lead to more compliant and flexible unit cells, hence lowering the modal frequencies and promoting more out-of-plane mode shapes in lower-order modes.

Based on our understanding of kerf parameters on the dynamic response of kerf unit cells, we have explored two large-scale kerf panels with different kerf cut patterns, i.e. uniform density and transitioning density kerf panels. We have demonstrated the need to introduce local flexibility through varying kerf cut density such as in the transitioning density kerf panel to reconfigure the kerf panels into a shape with high curvature regions in proximity. We used both beam element model and scanning laser vibrometry experiments to study the dynamic response of kerf panels. Both kerf panels show global out-of-plane motions in the earlier mode shapes. Whereas global in-plane motions are observed in the higher-order modes (>35). Due to varying kerf cut density across the panel, the transitioning kerf panel does not show paired modes. We have also studied the modal response of kerf structures reconfigured into local and global shapes. Both local and global reconfigurations of kerf panels with both uniform and

transitioning cut patterns influence the mode shapes significantly when compared to the mode shapes of flat panels. In the local perturbation, only a small region of the kerf panel is deformed, which leads to less change in the resonance frequencies compared to the globally reconfigured kerf panel.

We have explored the stress wave propagation in both flat and reconfigured (deformed) kerf panels under a localized impact loading. The kerf structures delay the propagation of stresses and vibrate for a longer time compared to the solid panel. The local vibration consumes the kinetic energy from the impact. As the stress is being attenuated during the propagation, the delay in wave propagation can further reduce the amplitude of stress when it propagates away from the impacted region. Due to the flexibility of kerf structures, the kerf panels can be easily reconfigured into a desired shape with low pre-deformation stresses and alter the stress wave propagation due to dynamic loading.

As kerf structures can be easily reconfigured into desirable shapes, they have the potential for tuning dynamic response and wave propagations in structures exposed to dynamic loading. These findings would lead to the designing of kerf structures with desired performance requirements; for example, in tuning the indoor acoustics, altering the wind response of the buildings in the outdoors, avoiding resonance in building facades, mitigating vibrations in morphing structures, and dissipating energy in structures exposed to impact loadings.

**Acknowledgments**

The authors are grateful to Vikrant and Florian at Polytec for assisting with the experiments. The authors acknowledge the Texas A&M Supercomputing Facility for providing computing resources that are used in conducting the research reported in this paper. AM and NK also acknowledged the support from the National Science Foundation under grants CMMI 1912823 and CMMI 1913688.

## 8. References


1. Nastri, M., *Future Façade Systems. Technological Culture and Experimental Perspectives*, in *Material Balance*. 2021, Springer. p. 83-103.
2. Nirmal, A.V.K., *Wind and Architecture: Design to the flow.* 2017.
3. Peters, B., et al., *Responsive acoustic surfaces: Computing sonic effects.* 2011.
4. Belanger, Z., W. McGee, and C. Newell, *Slumped Glass: Auxetics and Acoustics.* 2018.
5. Holterman, A., *Pattern Kerfing for Responsive Wooden Surfaces: A formal approach to produce flexible panels with acoustic performance.* 2018.
6. Zarrinmehr, S., et al., *Kerfing with generalized 2D meander-patterns: conversion of planar rigid panels into locally-flexible panels with stiffness control.* 2017.
7. Ivanisevic. *Super flexible laser cut plywood*. 2014; Available from: https://lab.kofaktor.hr/en/portfolio/super-flexible-laser-cut-plywood/.
8. Zarrinmehr, S., et al. *An Algorithmic Approach to Obtain Generalized 2D Meander-Patterns*. in *Bridges 2017 Conference Proceedings*. 2017. Tessellations Publishing.
9. Kalantar, N. and A. Borhani, *Informing Deformable Formworks-Parameterizing Deformation Behavior of a Non-Stretchable Membrane via Kerfing.* 2018.
10. Zarrinmehr, S., et al., *Interlocked archimedean spirals for conversion of planar rigid panels into locally flexible panels with stiffness control.* Computers & Graphics, 2017. **66**: p. 93-102.
11. Chen, R., et al., *Mechanics of kerf patterns for creating freeform structures.* Acta Mechanica, 2020: p. 1-26.
12. Shahid, Z., et al., *An investigation of the dynamic response of architectural kerf structures.* Acta Mechanica, 2022: p. 1-25.
13. Callens, S.J. and A.A. Zadpoor, *From flat sheets to curved geometries: Origami and kirigami approaches.* Materials Today, 2018. **21**(3): p. 241-264.
14. Chen, Y., R. Peng, and Z. You, *Origami of thick panels.* Science, 2015. **349**(6246): p. 396-400.
15. Lang, R.J., et al., *Thick rigidly foldable origami mechanisms based on synchronized offset rolling contact elements.* Journal of Mechanisms and Robotics, 2017. **9**(2): p. 021013.
16. Peraza-Hernandez, E.A., et al., *Origami-inspired active structures: a synthesis and review.* Smart Materials and Structures, 2014. **23**(9): p. 094001.
17. Boley, J.W., et al., *Shape-shifting structured lattices via multimaterial 4D printing.* Proceedings of the National Academy of Sciences, 2019. **116**(42): p. 20856-20862.
18. Clausen, A., et al., *Topology optimized architectures with programmable Poisson's ratio over large deformations.* Adv. Mater, 2015. **27**(37): p. 5523-5527.
19. Wang, F., O. Sigmund, and J.S. Jensen, *Design of materials with prescribed nonlinear properties.* Journal of the Mechanics and Physics of Solids, 2014. **69**: p. 156-174.
20. Soleimani, H., T. Goudarzi, and M. Aghdam, *Advanced structural modeling of a fold in Origami/Kirigami inspired structures.* Thin-Walled Structures, 2021. **161**: p. 107406.
21. Filipov, E.T., T. Tachi, and G.H. Paulino, *Origami tubes assembled into stiff, yet reconfigurable structures and metamaterials.* Proceedings of the National Academy of Sciences, 2015. **112**(40): p. 12321-12326.
22. Zelhofer, A.J. and D.M. Kochmann, *On acoustic wave beaming in two-dimensional structural lattices.* International Journal of Solids and Structures, 2017. **115**: p. 248-269.

23. Tee, K., et al., *Wave propagation in auxetic tetrachiral honeycombs.* Journal of Vibration and Acoustics, 2010. **132**(3).
24. Jenett, B., et al. *Meso-scale digital materials: modular, reconfigurable, lattice-based structures*. in *International Manufacturing Science and Engineering Conference*. 2016. American Society of Mechanical Engineers.
25. Popescu, A.M., *Vibrations Analysis of Discretely Assembled Ultra-Light Aero Structures*. 2019: eScholarship, University of California.
26. Bilal, O.R., A. Foehr, and C. Daraio, *Reprogrammable phononic metasurfaces.* Advanced materials, 2017. **29**(39): p. 1700628.
27. DARNAL, A., et al. *Viscoelastic Responses of MDF Kerf Structures*. in *Proceedings of the American Society for Composites—Thirty-Sixth Technical Conference on Composite Materials*. 2021.
28. Hibbett, Karlsson, and Sorensen, *ABAQUS/standard: User's Manual*. Vol. 1. 1998: Hibbitt, Karlsson & Sorensen.
29. SHAHID, Z., et al. *Dynamic Responses of Architectural Kerf Structures*. in *Proceedings of the American Society for Composites—Thirty-Sixth Technical Conference on Composite Materials*. 2021.
30. Potter, J.L., *Comparison of modal analysis results of laser vibrometry and nearfield acoustical holography measurements of an aluminum plate.* 2011.

## Appendix A

### Beam Model Formulation

In this study, $\theta = 60°$ creates a kerf panel with a triangular spiral pattern to form a hexagon kerf pattern (see **Fig. 2**). The folded beams are a combination of identical straight beams where $i = 1, 2, .. N + 1$, with $N$ folds connecting the beams at an arbitrary angle. The displacements for each beam segment ($i$) are:

$$u_1^{(i)}\left(x_1^{(i)}, t\right), u_2^{(i)}\left(x_1^{(i)}, t\right), u_3^{(i)}\left(x_1^{(i)}, t\right) \quad 0 \le x_1^{(i)} \le l^{(i)} \tag{A1}$$

To derive the equations of motion for the folded beams, continuity conditions at $x_1^{(i)} = l^{(i)}$ and $x_1^{(i+1)} = 0$ are used ($l^{(i)}$ is the length of each beam segment). The continuity conditions imply that the resultants of internal moments and forces are equal and the displacements are continuous at $x_1^{(i)} = l$ and $x_1^{(i+1)} = 0$. The displacement transformation and continuity condition used in the analysis are:

$$\begin{Bmatrix} u_1^{(i)}(l^{(i)}, t) \\ u_3^{(i)}(l^{(i)}, t) \end{Bmatrix} = \begin{bmatrix} -cos\theta & -sin\theta \\ sin\theta & -cos\theta \end{bmatrix} \begin{Bmatrix} u_1^{(i+1)}(0, t) \\ u_3^{(i+1)}(0, t) \end{Bmatrix}$$

$$u_2^{(i)}\left(l^{(i)}, t\right) = u_2^{(i+1)}(0, t) \tag{A2}$$

The slope continuity condition is:

$$\frac{\partial u_2^{(i)}}{\partial x_1^{(i)}}(l^{(i)}, t) = \frac{\partial u_2^{(i+1)}}{\partial x_1^{(i+1)}}(0, t);$$

$$\frac{\partial u_3^{(i)}}{\partial x_1^{(i)}}\left(l^{(i)}, t\right) = \frac{\partial u_3^{(i+1)}}{\partial x_1^{(i+1)}}(0, t) \tag{A3}$$

The continuity conditions for bending moments are:

$$E^{(i)} I_{22}^{(i)} \left(\frac{\partial \varphi_2^{(i)}(l^{(i)}, t)}{\partial x_1^{(i)}}\right) = E^{(i+1)} I_{22}^{(i+1)} \left(\frac{\partial \varphi_2^{(i+1)}(0, t)}{\partial x_1^{(i+1)}}\right);$$

$$E^{(i)} I_{33}^{(i)} \left(\frac{\partial \varphi_3^{(i)}(l^{(i)}, t)}{\partial x_1^{(i)}}\right) = E^{(i+1)} I_{33}^{(i+1)} \left(\frac{\partial \varphi_3^{(i+1)}(0, t)}{\partial x_1^{(i+1)}}\right) \tag{A4}$$

The continuity conditions for shear and normal forces are:

$$kG^{(i)}A^{(i)}\left(-\varphi_3^{(i)}\left(l^{(i)},t\right)+\frac{\partial u_2^{(i)}\left(l^{(i)},t\right)}{\partial x_1^{(i)}}\right)= kG^{(i+1)}A^{(i+1)}\left(-\varphi_3^{(i+1)}(0,t)+\frac{\partial u_2^{(i+1)}(0,t)}{\partial x_1^{(i+1)}}\right);$$

$$kG^{(i)}A^{(i)}\left(\varphi_2^{(i)}\left(l^{(i)},t\right)+\frac{\partial u_3^{(i)}\left(l^{(i)},t\right)}{\partial x_1^{(i)}}\right)=E^{(i+1)}A^{(i+1)}\frac{du_1^{(i+1)}(0,t)}{dx_1^{(i+1)}}sin\theta-$$

$$kG^{(i+1)}A^{(i+1)}\left(\varphi_2^{(i+1)}(0,t)+\frac{\partial u_3^{(i+1)}(0,t)}{\partial x_1^{(i+1)}}\right)cos\theta;$$

$$E^{(i)}A^{(i)}\frac{du_1^{(i)}\left(l^{(i)},t\right)}{dx_1^{(i)}}= E^{(i+1)}A^{(i+1)}\frac{du_1^{(i+1)}(0,t)}{dx_1^{(i+1)}}cos\theta+kG^{(i+1)}A^{(i+1)}\left(\varphi_2^{(i+1)}(0,t)+\right.$$

$$\left.\frac{\partial u_3^{(i+1)}(0,t)}{\partial x_1^{(i+1)}}\right)sin\theta; \tag{A6}$$

The continuity condition for twisting is:

$$G^{(i)}J^{(i)}\frac{\partial^2\beta^{(i)}}{\partial {x_1^{(i)}}^2}=G^{(i+1)}J^{(i+1)}\frac{\partial^2\beta^{(i+1)}}{\partial {x_1^{(i+1)}}^2} \tag{A7}$$

For the folded beams, these conditions **Equation (A2-A6)** are substituted in **Equation (2)** to determine the equations of motion. These are further solved numerically to determine the modal response of large-scale kerf structures (see **Fig. 2(c)**).

## Appendix B

**Torsional constant of beam segments of the unit cells**

During torsion, the ability of the beam to undergo twisting depends on the torsional constant of the beam, $J$ which is the sum of polar moment of area, $I_p$ and torsional constant due to warping, $I_w$. The torsional constant is determined using these equations:

$$I_p = \int_A ((x_2)^2 + (x_3)^2) dA$$

$$I_w = \int_A (-x_2 \frac{\partial \phi}{\partial x_3} + x_3 \frac{\partial \phi}{\partial x_2}) dA$$

$$J = I_p + I_w \quad \text{(B1)}$$

where, $\phi(x_2, x_3)$ is the warping function of the cross-section. We determined the torsional constant for beams in LD, MD, and HD unit cells as shown in **Table 2**. It is evident from the results that the beams in the LD unit cell have a higher torsional constant, $J$ compared to the HD unit cell beams which lead to the conclusion that the LD unit cell undergoes less twisting. During out-of-plane bending in the unit cells, the beams in the unit cell undergo both bending and twisting. The capability of the beams to undergo bending and twisting depends on the geometrical parameters of the beam. It can be noticed that in the out-of-plane bending, the beams in the HD unit cell majorly undergo twisting compared to bending as shown by the high ratio of $\frac{I_{33}}{J}$ relative to MD and LD unit cells. Whereas, the beams in LD unit cells are relatively thick so they dominantly undergo bending relative to twisting as shown by the low ratio of $\frac{I_{33}}{J}$.

Additionally, we also calculated torsional constants for beams in different sizes of unit cells (see **Table 3**). The larger unit cells have a higher torsional constant compared to smaller unit cells which lead to relatively less twisting in larger unit cells. In out-of-plane bending, the beams in larger unit cells dominantly undergo out-of-plane bending compared to twisting as shown by the low ratio of $\frac{I_{33}}{J}$ relative to smaller unit cells.

## Appendix C

### Modal experiments on kerf panels

In the modal experiments, the kerf panel is suspended from an aluminum frame using fishing lines. The free-free boundary conditions are chosen for the kerf panel specimens because it is relatively easier to implement free-free boundary conditions compared to other types of boundary conditions. The edges of the specimen are not constrained as shown in **Fig. C1** and it is ensured that the edges are free to move.

To experimentally determine the mode shapes and frequencies of the kerf panels, scanning laser vibrometry is chosen as it is a non-contact measurement technique [30]. The scanning vibrometer (PSV-500, Polytec, Irvine, CA) is used to measure the modal frequencies and shapes as shown in **Fig. C1**. The Automatic Modal Hammer (SAM1, Polytec, Irvine, CA) is used to actuate the specimen as it allows precise excitation without mass loading. The excitation point is carefully chosen near the bottom edge of the kerf panel and it is kept the same for all the tests. The scanning vibrometer is used to perform the modal analysis with the force input of 50 N from the modal hammer.

In the case of a uniform kerf panel, the velocity output range for the vibrometer is kept at 125 mm/s with a sampling rate of 2.5 kHz. A Fast Fourier Transform (FFT) is performed within a selected bandwidth of 156 mHz – 1000 Hz. It is necessary to choose sufficient measurement points to capture the motion of all the segments in the kerf structures so based on experience from previous tests [12], 1401 measurement points are chosen on the surface of uniform kerf panel. Whereas, for the transitioning kerf specimen, the velocity output range for scanning laser vibrometer is kept at 250 mm/s. The sampling rate is 2.5 kHz and the bandwidth for FFT is kept 78.125 mHz - 1000 Hz. A total of 1025 points on the surface of the transitioning kerf specimen are used as measurement locations, each scanning point and FFT is averaged 3 times. The Frequency Response Function (FRF) for each data point is obtained and stored in a

file that is post-processed in the PSV software (Polytec, Irvine, CA) to extract mode shapes and resonance frequencies.

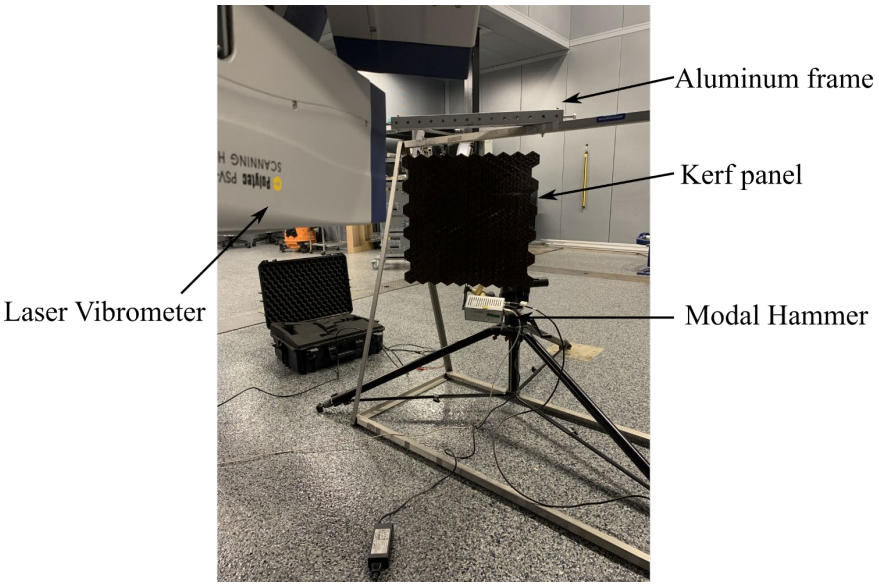


**Fig. C1 Experimental test set-up for modal testing of kerf panels**

**The discrepancy between model and experimental results at higher frequencies**

At higher modes (>11) of the kerf panels, there is a discrepancy between model and experimental results. During the measurements at higher frequencies (>200 Hz), we observe several local regions on the kerf panel undergoing microscopic deformations as opposed to macroscopic deformations observed in earlier modes shapes (<10). For example, **Fig. C2** shows a higher order mode extracted from the laser vibrometry experiment performed on a uniform density kerf panel in which numerous regions of the panel are undergoing microscopic deformations. With the finite number of measurement points on the kerf surface chosen as mentioned above, it becomes difficult for the laser vibrometer to capture all the deformations in the higher mode shapes. Whereas the beam element model can capture all the deformations during both in-plane and out-of-plane motion in the higher order modes. Another reason for the discrepancies is due to possible slight imperfections in the cuts around the corners,

especially in the regions which have high density cut lines. The beam element model of the panel disregards any kind of imperfections caused by cutting.

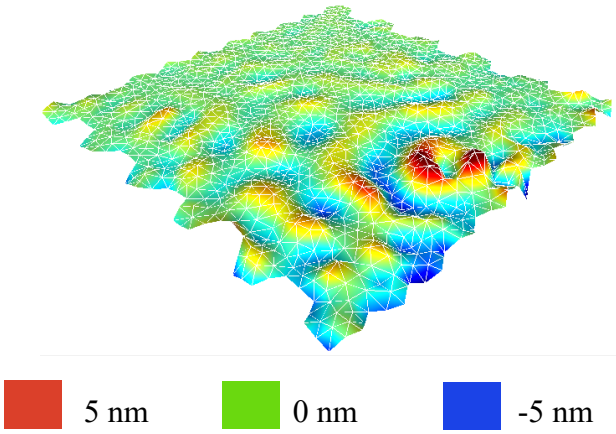


**Fig. C2 Higher order mode extracted from laser vibrometry experiment on uniform density kerfing panel, at frequency 220 Hz**

Similarly, in the kerf unit cells at higher order modes (>8), the discrepancy between model and experimental results increases. At higher frequencies (>4000 Hz), the noise becomes dominant in the experimental results which makes it intricate to determine distinct natural frequencies and mode shapes (see **Fig. C3**).

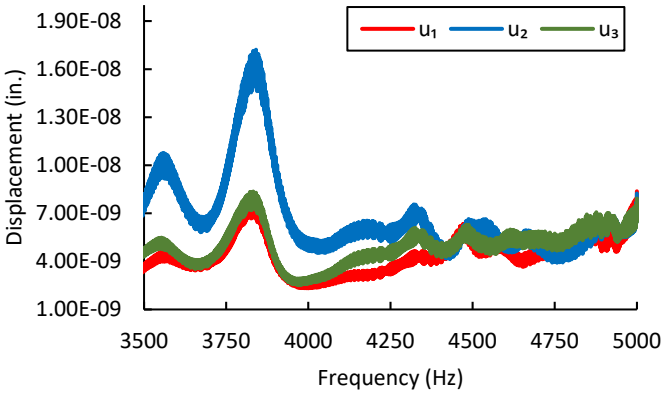


**Fig. C3 Results from laser vibrometry experiment on LD unit cell showing dominant noise in the data above 4000 Hz**

## Appendix D

### Influences of pre-deformation stresses

To understand the influence of stresses due to local and global shape reconfiguration of the kerf panels, we compared the modal response of the kerf panel with and without taking stresses due to the pre-deformation into consideration.

In the first case, the transitioning density kerf panel is globally deformed by prescribing a 0.4 out-of-plane displacement at three high density cut regions to form a shape with multiple high curvatures. It can be noticed from the results in **Fig. D1** that the modal behavior is significantly influenced by pre-deformation stresses in this case. The root mean square error (RMSE) between resonance frequencies for the deformed kerf panel with and without pre-deformation stresses is 10.79 Hz, which is high compared to the magnitude of natural frequencies. Reconfiguring the kerf panel with multiple high curvatures induces stresses in multiple neighboring unit cells around the actuated region as shown in **Fig. D1**. These pre-existing stresses have a significant effect on the dynamics response of large-scale kerf structures.

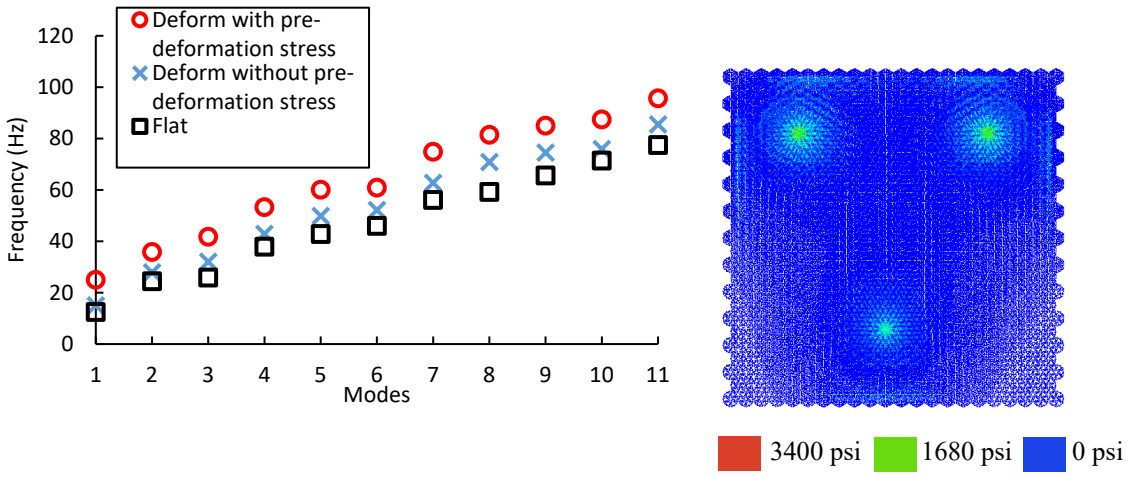


**Fig.D1 Comparison of modal frequencies of molded transitioning kerf panel (multiple high curvatures) with and without pre-deformation stresses (left); von-Mises stresses in molded transitioning kerf panel (right)**

In the second case, the uniform density kerf panel is locally perturbed at the center by prescribing 0.04 in. out-of-plane displacement. It can be noticed from the results in **Fig. D2** that the effect of pre-deformation stresses on the modal response is negligible. The root mean square error (RMSE) between resonance frequencies for the deformed kerf panel with and without pre-deformation stresses is 0.0006 Hz, which is negligible compared to natural frequencies. Locally perturbing the kerf panel induces stresses in a small region of the kerf panel as shown in **Fig. D2**, which leads to an insignificant effect of pre-deformation stresses on the dynamics response of large-scale kerf structures.

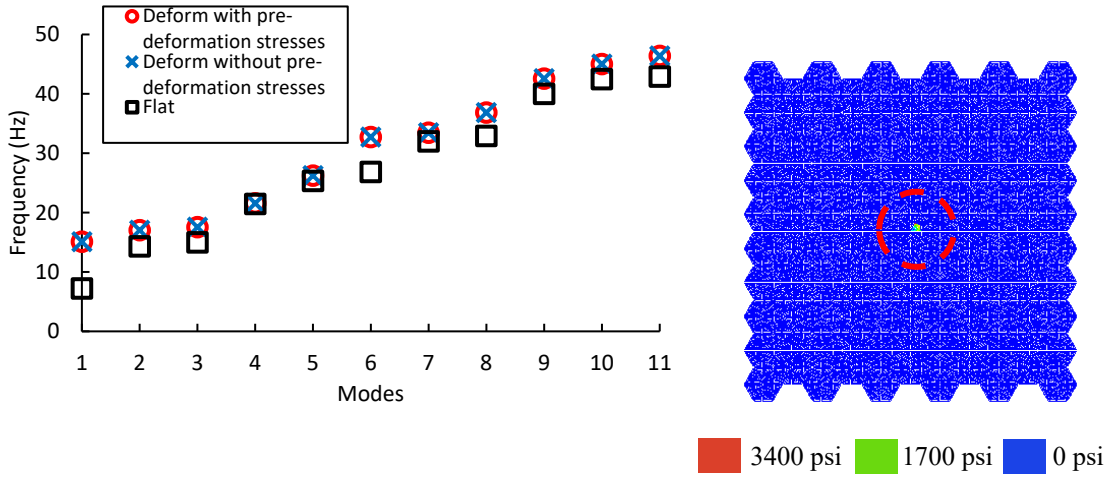


**Fig.D2 Comparison of modal frequencies of molded uniform kerf panel (local perturbation) with and without pre-deformation stresses (left); von-Mises stresses in molded uniform kerf panel (right)**

## Appendix E

### Influences of material behaviors

To understand the influence of the delayed responses (viscoelastic dissipation) of the materials on the stress wave propagation in a kerf panel, we consider an impact loading in Eq. (6) with different rates, i.e., 0.005 sec and 0.05 sec. An MDF panel with a uniform cut density is considered in the analyses. It is seen in Fig. E1 that the rate of stress decay changes when the kerf panel is exposed to different impact rates. A slower loading yields a more pronounced effect of the delayed responses of the materials (viscoelastic effect). Faster loadings will minimize the viscoelastic effect as the responses are more dominated by the instantaneous elastic behavior of the materials.

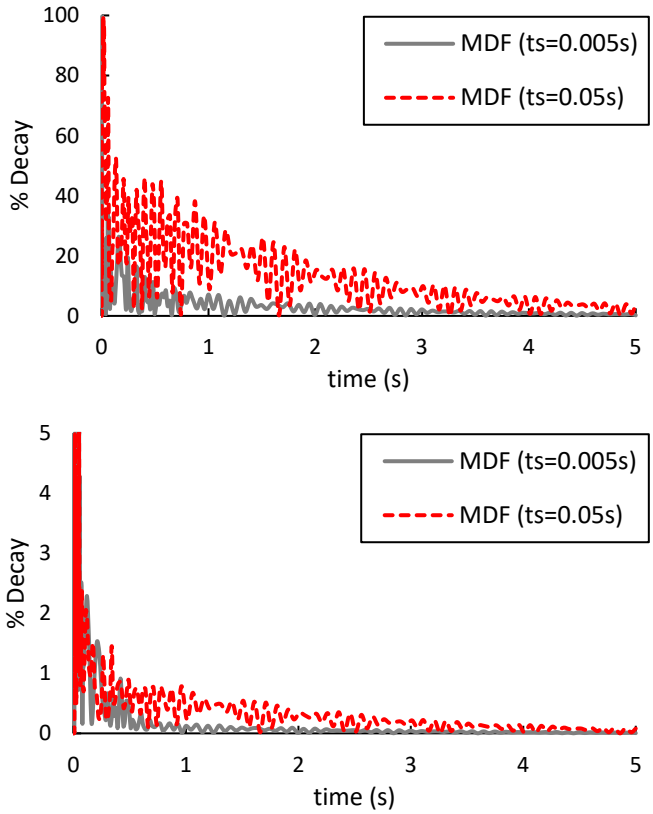


**Fig. E.1 Comparison of stress decay in a kerf panel in the center (top) and top left corner (bottom) exposed to different rates of impact loading**

To further examine the effect of material behaviors, a uniform cut density kerf panel made of stainless steel (SS) material is subjected to an impact loading, following Eq. (6). The metallic panels when loaded below the yield limit of the material can be considered as made up of an elastic material. The elastic properties of the SS were obtained from our previous study [12]. The stress decay rate in the SS kerf panel is comparable to the MDF kerf panel, indicating that the kerf geometries contribute to the delayed stress wave propagation (Fig. E2). It is also seen that the elastic SS kerf panel experiences a faster stress decay compared to the viscoelastic MDF kerf panel because there is no delayed response of the materials.

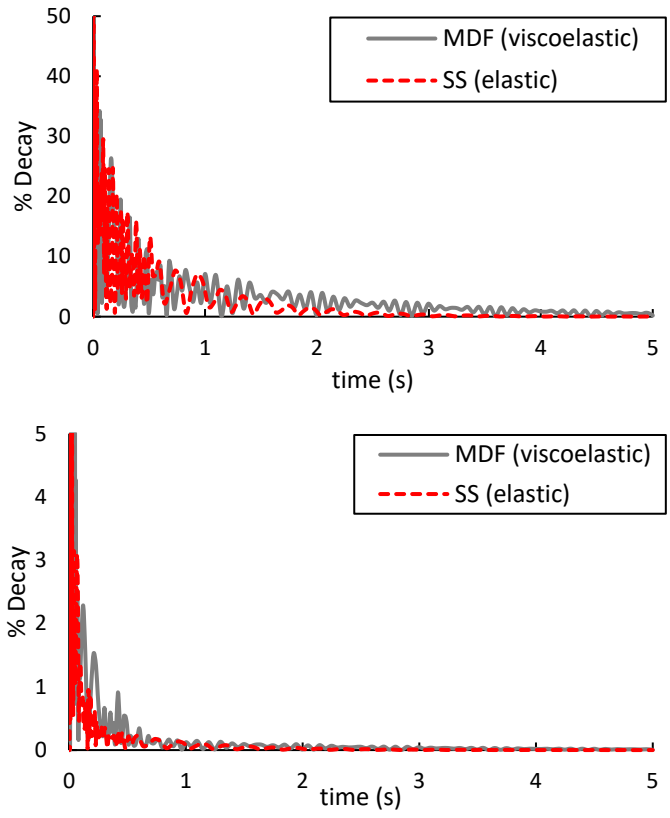


**Fig. E.2 Comparison of stress decay in a kerf panel made up of SS and MDF in the center (top) and top left corner (bottom) exposed to an impact loading with a rate of 0.005 sec**